

Supporting Information

Photocatalytic and electrocatalytic hydrogen production using nickel complexes supported by hemilabile and non-innocent ligands

Satoshi Inoue,^a Yin-Nan Yan,^a Katsunori Yamanishi,^a Yusuke Kataoka,^b and Tatsuya Kawamoto*^a

^aDepartment of Chemistry, Faculty of Science, Kanagawa University, 2946 Tsuchiya, Hiratsuka, Japan

Email: kaw@kanagawa-u.ac.jp

^bDepartment of Material Science, Interdisciplinary Graduate School of Science and Engineering, Shimane University, 1060 Nishikawatsu, Matsue, 690-8504, Japan.

EXPERIMENTAL SECTION

General.

Reagents and solvents were purchased from commercial sources and used without further purification. The ligand **PyBtH₂** and Ni complex **1a** were synthesized following our previous report.¹ [Ir(ppy)₂(bpy)]PF₆ and [Ir(ppy)₂(dtbbpy)]PF₆ were prepared following a procedure slightly modified from that reported by Bernhard et al.² [4](ClO₄)₂ was synthesized on the basis of a method reported by Patra et al.³ CHN elemental analyses were performed by a PerkinElmer 2400 series II CHNS/O analyzer. ¹H NMR spectra were collected on a JEOL JMN-ECA 400 NMR spectrometer and referenced to tetramethylsilane for acetone-*d*₆ and the residual proton peak of the solvent for CD₃CN. UV-vis-NIR spectra were recorded on a JASCO V-570 spectrophotometer using a quartz cuvette (light path length = 1 cm). Single-crystal X-ray diffraction data were collected at 200 K on a Rigaku VariMax with Saturn diffractometer. Crystals were placed in the loop with parabar oil and mounted on the X-ray diffractometer. Structures were solved using SIR2004^{4a}, SIR2008^{4b}, or SHELXT Version 2018/2^{5a} and refined using SHELXL-97 or SHELXL Version 2018/3^{5b}. All non-hydrogen atoms were refined anisotropically. All hydrogen atoms were placed in ideal positions and refined isotropically. All calculations were performed using CrystalStructure software package.⁶ IR spectra were recorded on a JASCO FT/IR-4100 spectrometer as KBr disks. ESR spectra were collected on a JEOL JES-RE2X ESR spectrometer.

Synthesis of 2-(Pyridin-2-yl)benzothiazoline (PyBtH₂).

To a solution of 2-aminobenzenethiol (1.29 g, 10.3 mmol) in ethanol (30 mL) was added pyridine-2-carbaldehyde (0.986 mL, 10.3 mmol), and the solution was refluxed under N₂ atmosphere for 2 h. The reaction solution was concentrated until a solid formed, and then addition of hexane (30 mL) was followed by cooling with vigorous stirring to give a further solid product. After the liquid phase was removed by decantation, the residual pale yellow powder was washed with cold hexane (3 × 30 mL). The resulting off-white powder was collected by filtration and dried in vacuo. Yield: 1.95 g, 88.5%. Elem. Anal. Calcd for C₁₂H₁₀N₂S: C, 67.26; H, 4.70; N, 13.07. Found: C, 67.32; H, 4.66; N, 13.11. ¹H NMR (400 MHz, CD₃CN): δ 5.60 (brs, 1H, NH), 6.35 (d, *J* = 3.3 Hz, 1H, bt-H2), 6.69 (ddd, *J* = 7.6, 7.5 and 1.1 Hz, 1H, bt-H6), 6.74 (dd, *J* = 7.7 and 1.1 Hz, 1H, bt-H4), 6.94 (ddd, *J* = 7.7, 7.6 and 1.3 Hz, 1H, bt-H5), 7.00 (d with fine coupling, *J* = 7.5 Hz, 1H, bt-H7), 7.25 (ddd, *J* = 7.6, 4.8 and 1.1 Hz, 1H, py-H5), 7.53 (d with fine coupling, *J* = 7.9 Hz, 1H, py-H3), 7.75 (ddd, *J* = 7.9, 7.6 and 1.8 Hz, 1H, py-H4), 8.50 (ddd, *J* = 4.8, 1.8 and 0.9 Hz, 1H, py-H6) ppm. IR (KBr): 3194 (s, N-H), 3069 (m), 2876 (m), 1590 (s), 1469 (s), 1436 (m), 750 (s) cm⁻¹.

Synthesis of 5-Chloro-2-(pyridin-2-yl)benzothiazoline (PyClBtH₂).

PyClBtH₂ was synthesized following the same procedure described for **PyBtH₂** using 2-amino-4-chlorobenzenethiol (4.06 g, 25.5 mmol) and pyridine-2-carbaldehyde (2.44 mL, 25.5 mmol) instead of 2-aminobenzenethiol and pyridine-2-carbaldehyde. The product was obtained as a pale orange powder. Yield: 5.37 g, 84.7%. Elem. Anal. Calcd for C₁₂H₉ClN₂S: C, 57.94; H, 3.65; N, 11.26. Found: C, 57.79; H, 3.55; N, 11.30. ¹H NMR (400 MHz, CD₃CN): δ 5.79 (brs, 1H, NH), 6.40 (d, *J* = 2.5 Hz, 1H, bt-H2), 6.65 (dd, *J* = 8.1 and 2.0 Hz, 1H, bt-H6), 6.70 (d, *J* = 2.0 Hz, 1H, bt-H4), 6.93 (d, *J* = 8.1 Hz, 1H, bt-H7), 7.26 (ddd, *J* = 7.6, 4.8 and 1.1 Hz, 1H, py-H5), 7.51 (d with fine coupling, *J* = 7.8 Hz, 1H, py-H3), 7.76 (ddd, *J* = 7.8, 7.6 and 1.8 Hz, 1H, py-H4), 8.50

(ddd, $J = 4.8, 1.8$ and 0.9 Hz, 1H, py-H6) ppm. IR (KBr): 3194 (s, N–H), 2928 (w), 2876 (w), 1582 (s), 1456 (s), 1436 (s), 1347 (m), 1076 (s), 839 (m), 803 (s), 748 (s) cm^{-1} .

Synthesis of 2-(Pyridin-2-yl)-5-(trifluoromethyl)benzothiazoline (PyCF₃BtH₂).

To hot ethanol (100 mL) containing NaOH (0.829 g, 20.7 mmol) were added 2-amino-4-(trifluoromethyl)benzenethiol hydrochloride (4.91 g, 21.4 mmol) and pyridine-2-carbaldehyde (1.98 mL, 20.7 mmol). The mixture was refluxed under N₂ atmosphere for 5 h, and then cooled to room temperature. After the suspension was filtered to remove a white solid, the filtrate was concentrated until a solid formed. To the mixture was added hot hexane (150 mL) followed by cooling with stirring to give a further solid product. The liquid phase was removed by decantation, and the residual pale yellow powder was washed with cold hexane (3 × 20 mL). The powder was collected by filtration and dried in vacuo. The obtained crude product was put into dichloromethane (30 mL), and then a residual solid was removed by filtration. The filtrate was evaporated to dryness and dried in vacuo to afford a pale orange powder. Yield: 3.13 g, 53.6%. Elem. Anal. Calcd for C₁₃H₉F₃N₂S: C, 55.31; H, 3.21; N, 9.92. Found: C, 55.34; H, 2.97; N, 9.97. ¹H NMR (400 MHz, CD₃CN): δ 5.91 (brs, 1H, NH), 6.46 (d, $J = 2.7$ Hz, 1H, bt-H2), 6.92 (s, 1H, bt-H4), 6.95 (ddd, $J = 7.9, 1.7$ and 0.8 Hz, 1H, bt-H6), 7.12 (d, $J = 7.9$ Hz, 1H, bt-H7), 7.27 (ddd, $J = 7.6, 4.8$ and 1.1 Hz, 1H, py-H5), 7.51 (d with fine coupling, $J = 7.8$ Hz, 1H, py-H3), 7.77 (ddd, $J = 7.8, 7.6$ and 1.7 Hz, 1H, py-H4), 8.51 (ddd, $J = 4.8, 1.7$ and 0.9 Hz, 1H, py-H6) ppm. IR (KBr): 3188 (m, N–H), 2891 (w), 1596 (m), 1459 (m), 1333 (s, C–F), 1246 (m), 1161 (s, C–F), 1112 (s, C–F), 1074 (s), 820 (m) cm^{-1} .

Synthesis of 1,2-Bis(2-aminophenylthio)ethane (BAPTE).

BAPTE was prepared following a procedure modified from that described in the literature.⁷ To a solution of NaOH (979 mg, 24.5 mmol) in ethanol (100 mL) were added 1,2-dibromoethane (1.10 mL, 12.9 mmol) and 2-aminobenzenethiol (3.00 g, 24.0 mmol). After the solution was refluxed under N₂ atmosphere for 15 h, ethanol (70 mL) was added to the reaction mixture, and the resulting suspension was heated until the reaction product dissolved. The solution was poured into cold water (300 mL) and the mixture was cooled. The resulting solid was collected by filtration and well dried in vacuo. The crude product was put into hot hexane (230 mL) and an oily layer was below the hexane layer. While the mixture was kept hot, the hexane layer was collected by decantation, and then cooled in a refrigerator overnight to give a pale yellow crystalline solid. This solid was collected by filtration, washed with a small amount of cold hexane, finely crushed and dried in vacuo. The desired product was obtained as a pale yellow powder. Yield: 1.80 g, 54.2%. Elem. Anal. Calcd for C₁₄H₁₆N₂S₂: C, 60.83; H, 5.83; N, 10.13. Found: C, 60.91; H, 5.87; N, 10.12. ¹H NMR (400 MHz, CD₃CN): δ 2.81 (s, 4H, CH₂), 4.63 (brs, 4H, NH₂), 6.57 (ddd, $J = 7.7, 7.3$ and 1.4 Hz, 2H, ph-H5), 6.71 (dd, $J = 8.2$ and 1.4 Hz, 2H, ph-H3), 7.07 (ddd $J = 8.2, 7.3$ and 1.8 Hz, 2H, ph-H4), 7.24 (dd, $J = 7.7$ and 1.8 Hz, 2H, ph-H6) ppm. IR (KBr): 3388 (s, N–H), 3361 (s, N–H), 3295 (s), 1620 (s), 1479 (s), 1447 (s), 1305 (m), 1206 (m), 858 (m), 750 (s), 698 (m), 467 (m) cm^{-1} .

Synthesis of 1,2-Bis[2-(pyridin-2-ylmethyleneamino)phenylthio]ethane (BPAPTE).

BPAPTE was synthesized according to previous report.⁸ BAPTE (803 mg, 2.90 mmol) and pyridine-2-carbaldehyde (0.560 mL, 5.86 mmol) in dry ethanol (30 mL) were refluxed under N₂ atmosphere for 4 h. The

solvent was removed under rotary evaporation and the oily residue was dissolved in hot dry acetonitrile (20 mL). The resulting solution was cooled in a refrigerator overnight to afford a precipitate. After removal of the mother liquor by decantation, the residual yellow powder was washed with cold dry acetonitrile (3 × 30 mL), collected by filtration and dried in vacuo. Yield: 873 mg, 66.2%. Elem. Anal. Calcd for C₂₆H₂₂N₄S₂: C, 68.69; H, 4.88; N, 12.32. Found: C, 68.64; H, 4.94; N, 12.31. ¹H NMR (400 MHz, CD₃CN): δ 3.19 (s, 4H, CH₂), 7.13 (dd, *J* = 7.6 and 1.6 Hz, 2H, ph-H₃), 7.19 (ddd, *J* = 7.6, 7.4 and 1.6 Hz, 2H, ph-H₅), 7.25 (ddd, *J* = 7.6, 7.4 and 1.5 Hz, 2H, ph-H₄), 7.32 (dd, *J* = 7.6 and 1.5 Hz, 2H, ph-H₆), 7.44 (ddd, *J* = 7.6, 4.8 and 1.3 Hz, 2H, py-H₅), 7.86 (ddd, *J* = 7.8, 7.6 and 1.7 Hz, 2H, py-H₄), 8.13 (ddd, *J* = 7.8, 1.3 and 1.0 Hz, 2H, py-H₃), 8.46 (s, 2H, CHN), 8.68 (ddd, *J* = 4.8, 1.7 and 1.0 Hz, 2H, py-H₆) ppm. IR (KBr): 3059 (w), 2919 (w), 1622 (m, C=N), 1565 (m), 1473 (s), 1435 (m), 1262 (m), 775 (s), 735 (s), 493 (m) cm⁻¹.

Synthesis of [Ni(pybt)₂] (1a).

To a solution of **PyBtH₂** (304 mg, 1.42 mmol) in ethanol (20 mL) was added Ni(OAc)₂·4H₂O (173 mg, 0.694 mmol). The mixture was refluxed under N₂ atmosphere for 1 h, and then cooled to room temperature. The resultant solid was collected by filtration, washed with ethanol (3 × 20 mL) and dried in vacuo to obtain as a dark blue powder. Yield: 246 mg, 73.1%. Black block crystals suitable for single-crystal X-ray analysis were obtained by layering diethyl ether over *N,N*-dimethylformamide solution under ambient conditions. Elem. Anal. Calcd for C₂₄H₁₈N₄NiS₂: C, 59.40; H, 3.74; N, 11.55. Found: C, 59.19; H, 3.63; N, 11.36. UV-vis (DMF) λ_{max} (ε_M/M⁻¹ cm⁻¹) 608 (6630) nm. IR (KBr): 3044 (w), 1599 (m, C=N), 1472 (s), 1447 (s), 1282 (m), 1119 (s), 1065 (s), 775 (s), 742 (s), 712 (m) cm⁻¹.

Synthesis of [Ni(pyClbt)₂] (2a).

2a was synthesized following the same procedure described for **1a** using **PyClbtH₂** (313 mg, 1.26 mmol) and Ni(OAc)₂·4H₂O (156 mg, 0.627 mmol). The product was obtained as a dark blue powder. Yield: 322 mg, 92.7%. Black block crystals suitable for single-crystal X-ray diffraction analysis were obtained by vapor diffusion of diethyl ether to *N,N*-dimethylformamide solution under ambient conditions. Elem. Anal. Calcd for C₂₄H₁₆Cl₂N₄NiS₂: C, 52.02; H, 2.91; N, 10.11. Found: C, 52.01; H, 2.94; N, 9.96. UV-vis (DMF) λ_{max} (ε_M/M⁻¹ cm⁻¹) 613 (5875) nm. IR (KBr): 3047 (w), 1601 (m, C=N), 1472 (s), 1447 (s), 1229 (m), 1173 (m), 1127 (m), 1095 (s), 1060 (s), 933 (m), 771 (m), 609 (m) cm⁻¹.

Synthesis of [Ni(pyCF₃bt)₂] (3a).

3a was synthesized following the same procedure described for **1a** using **PyCF₃BtH₂** (509 mg, 1.80 mmol) and Ni(OAc)₂·4H₂O (224 mg, 0.899 mmol). The product was obtained as a dark violet powder. Yield: 535 mg, 95.9%. Black plate crystals suitable for single-crystal X-ray diffraction analysis were obtained by vapor diffusion of acetone to *N,N*-dimethylformamide solution under ambient conditions. Elem. Anal. Calcd for C₂₆H₁₆F₆N₄NiS₂: C, 50.26; H, 2.60; N, 9.02. Found: C, 50.12; H, 2.72; N, 8.94. UV-vis (DMF) λ_{max} (ε_M/M⁻¹ cm⁻¹) 571 (6305), 307 (49476) nm. IR (KBr): 3052 (w), 1598 (m, C=N), 1477 (m), 1322 (vs, C-F), 1255 (m), 1230 (m), 1163 (s), 1104 (s, C-F), 1084 (s, C-F), 941 (m), 771 (m), 499 (m) cm⁻¹.

Synthesis of [Ni(bpapte)](ClO₄)₂ ([5](ClO₄)₂).

[5](ClO₄)₂ was synthesized following the same procedure described in the literature.² Ni(ClO₄)₂·6H₂O (248 mg, 0.677 mmol) was dissolved in dry acetonitrile (50 mL), to which was added **BPAPTE** (312 mg, 0.686 mmol). The mixture was stirred at room temperature under N₂ atmosphere for 4 h, and then the solvent was evaporated to afford an oil. After this oil was dissolved in dry acetonitrile (30 mL) followed by filtration to remove a residue, to the filtrate was added diethyl ether (200 mL). The resultant brown powder was collected by filtration, washed with a small amount of diethyl ether and dried in vacuo. Yield: 408 mg, 84.6%. Orange block crystals suitable for single-crystal X-ray diffraction analysis were obtained by layering diethyl ether over acetonitrile solution under ambient conditions. Elem. Anal. Calcd for C₂₆H₂₂Cl₂N₄NiO₈S₂: C, 43.84; H, 3.11; N, 7.87. Found: C, 43.58; H, 3.10; N, 7.67. UV-vis (DMF) λ_{max} (ε_M/M⁻¹ cm⁻¹) 370 (13999) sh, 350 (24214), 335 (25319), 321 (22227) sh nm. IR (KBr): 3060 (w), 3009 (w), 2912 (w), 1595 (s, C=N), 1480 (s), 1144 (vs, Cl=O), 1117 (vs, Cl=O), 1089 (vs, Cl=O), 783 (s), 628 (s) cm⁻¹.

Chemical One-Electron Reduction of [Ni(pybt)₂] ([CoCp*₂][1b]·0.5CH₂Cl₂).

1a (100 mg, 0.207 mmol) was dissolved in dry *N,N*-dimethylformamide (120 mL) and the solution was degassed by freeze-pump-thaw cycling. To the solution was added decamethylcobaltocene (CoCp*₂; 69.2 mg, 0.210 mmol) and the mixture was stirred at 50 °C under N₂ atmosphere for 1 h. The solution was evaporated with heating at 50 °C and well dried in vacuo to give a deep green residue. To the crude product was added 1:10 (v/v) dichloromethane/acetone mixed solvent (11 mL), and then the mixture was filtered and the residue was washed with acetone (2 × 2 mL). After the combined filtrate was evaporated to dryness, the product was extracted with acetone (4 × 0.5 mL). The combined extract was evaporated to dryness and well dried in vacuo to afford a deep green solid. Yield, 163 mg, 91.8%. Black plate crystals suitable for single-crystal X-ray analysis were obtained by vapor diffusion of pentane to dichloromethane solution at room temperature under N₂ atmosphere. All solvents were preliminarily degassed by freeze-pump-thaw cycling and treated under N₂ atmosphere by using a Schlenk-and-syringe technique. Elem. Anal. Calcd for C₄₄H₄₈CoN₄NiS₂·C_{0.5}HCl: C, 62.36; H, 5.76; N, 6.54. Found: C, 62.46; H, 5.98; N, 6.67. UV-vis-NIR (DMF) λ_{max} (ε_M/M⁻¹ cm⁻¹) 1925 (399), 1762 (1869), 1415 (625), 913 (9487), 695 (2539), 401 (5824) sh nm. ¹H NMR (400 MHz, acetone-*d*₆): δ 1.77 (s, 30H, [CoCp*₂]⁺) (distinct signals are not observed except a signal for protons of [CoCp*₂]⁺ ppm. IR (KBr): 3036 (w), 2978 (w), 2911 (w), 1586 (m), 1468 (s), 1431 (s), 1376 (m), 1303 (s), 1151 (m), 1022 (m), 742 (s) cm⁻¹.

Chemical One-Electron Reduction of [Ni(pyClbt)₂] ([CoCp*₂][2b]·0.5CH₂Cl₂).

[CoCp*₂][**2b**] was obtained following the same procedure described for [CoCp*₂][**1b**] using **2a** (116 mg, 0.210 mmol) and CoCp*₂ (67.9 mg, 0.206 mmol). To the crude product was added 1:2 (v/v) dichloromethane/acetone mixed solvent (30 mL), which was concentrated to a half of the initial volume. The mixture was filtered and the residue was washed with acetone (10 × 2 mL), and then the combined filtrate was evaporated to dryness to afford a deep green solid. The solid was washed with acetone (5 × 0.5 mL) and dried in vacuo. Yield, 95.3 mg, 50.0%. Black plate crystals suitable for single-crystal X-ray analysis were obtained by the same method as described for [CoCp*₂][**1b**]. Elem. Anal. Calcd for C₄₄H₄₆Cl₂CoN₄NiS₂·C_{0.5}HCl: C, 57.72; H, 5.12; N, 6.05. Found: C, 57.71; H, 5.18; N, 6.17. UV-vis-NIR (DMF) λ_{max} (ε_M/M⁻¹ cm⁻¹) 1927 (875), 1761 (2204), 1407 (876), 934 (14681), 692 (3363), 398 (5882) nm. ¹H NMR (400 MHz, acetone-*d*₆): δ 1.78 (s, 30H, [CoCp*₂]⁺) (distinct signals are not observed except a signal for protons of [CoCp*₂]⁺ ppm. IR (KBr): 3042 (w), 2979 (w), 2912 (w), 1586 (m), 1550

(m), 1523 (s), 1469 (m), 1431 (m), 1306 (s), 1280 (s), 1076 (m), 963 (s), 790 (m) cm^{-1} .

Chemical One-Electron Reduction of [Ni(pyCF₃bt)₂] ([CoCp*₂][3b]·0.3CH₂Cl₂).

[CoCp*₂][3b] was prepared following the same procedure described for [CoCp*₂][1b] using 3a (132 mg, 0.213 mmol) and CoCp*₂ (70.0 mg, 0.213 mmol). The product was obtained as a deep green powder. Yield: 179 mg, 85.9%. Elem. Anal. Calcd for C₄₆H₄₆CoF₆N₄NiS₂·C_{0.3}H_{0.6}Cl_{0.6}: C, 56.97; H, 4.81; N, 5.74. Found: C, 57.03; H, 5.04; N, 5.49. UV-vis-NIR (DMF) λ_{max} ($\epsilon_{\text{M}}/\text{M}^{-1} \text{cm}^{-1}$) 1927 (433), 1782 (1374), 1422 (409), 890 (8100), 688 (1930), 480 (2137) sh, 435 (3072) sh, 387 (5983) sh, 343 (10926) sh nm. ¹H NMR (400 MHz, acetone-*d*₆): δ 1.80 (s, 30H, [CoCp*₂]⁺) (distinct signals are not observed except a signal for protons of [CoCp*₂]⁺) ppm. IR (KBr): 3048 (w), 2982 (w), 2914 (w), 1586 (m), 1474 (s), 1431 (s), 1322 (vs, C–F), 1270 (vs, C–F), 1107 (vs, C–F), 970 (s), 713 (m) cm^{-1} .

Photocatalytic Water Reduction to Molecular Hydrogen.

For quantitation of hydrogen evolved by photocatalytic water reduction, all of the reactions were carried out in a closed circular system equipped with single auto gas sampler produced by Makuhari Rikagaku Garasu Inc. and the irradiation was carried out with an Ushio Optical ModuleX 500 W xenon lamp with a longpass filter ($\lambda > 400$ nm). Evolved hydrogen was quantitated using a Shimadzu GC-8A gas chromatograph equipped with molecular sieve 5A stainless columns (3.0 mm I.D. \times 3.0 m \times 2) and a thermal conductivity detector (TCD).

A total of 10 mL of sample solution containing a WRC, a PS, a SED and water in DMF was prepared. The solution was degassed by freeze-pump-thaw with Schlenk techniques, and then transferred into a cell for photoreaction in a glovebox filled with Ar gas. After the cell was attached to the closed circular system, a cycle of degassing the headspace of the system with a vacuum pump followed by backfilling it with Ar gas was repeated four times, and finally the gas pressure in the system was adjusted to ca. 300 Torr with Ar gas. The reaction progressed by irradiation to the sample solution using the xenon lamp with magnetic stirring for 24 h at 25 °C. During the reaction, hydrogen evolved in the headspace of the closed circular system was quantitated with gas chromatography per 1 h.

Photosensitizer Emission Quenching Experiment.

Emission spectra were recorded by exciting the samples at 377 nm using a JASCO FP-8300 spectrofluorometer. A sample solution containing a PS in dry DMF and a stock solution containing a quencher in dry DMF were prepared. All solutions were degassed by freeze-pump-thaw cycling with Schlenk techniques prior to use. The sample solution was placed in a quartz cuvette sealed with a silicone rubber septum and filled with N₂ gas, and then purged with N₂ gas for 10 min. The concentration of the quencher in the sample solution in the cuvette was increased by injecting an aliquot of the stock solution using microsyringe. The change in the intensities of emission peak by increase in the quencher were monitored by collection of the spectra.

Cyclic Voltammetry (CV).

Measurement was performed with a CH Instruments model 620A electrochemical analyzer using a glassy carbon working electrode (diameter = 3.0 mm), a platinum wire auxiliary electrode and a saturated calomel reference electrode (SCE). The glassy carbon electrode was polished and washed thoroughly before measurement. A

sample solution containing nickel complex and $n\text{Bu}_4\text{NClO}_4$ as an electrolyte in dry DMF was prepared. For electrocatalytic proton reduction, to the sample solution was added an aliquot of acetic acid as a proton source using a microsyringe. In the study of the concentration dependence of nickel complex for electrocatalytic proton reduction, a solution containing nickel complex, $n\text{Bu}_4\text{NClO}_4$ and acetic acid in dry DMF was diluted with an aliquot of a stock solution containing the same concentrations of $n\text{Bu}_4\text{NClO}_4$ and acetic acid in the same solvent and was used as the sample solution. In all cases, the sample solution was well purged with N_2 gas before measurement.

Chemical Re-Oxidation of $[\text{CoCp}^*_2][\mathbf{1b}]$.

$[\text{CoCp}^*_2][\mathbf{1b}]$ (1.33 mg, 1.55 μmol) was dissolved in a small amount of acetone. A solution containing 1.0 equivalent of $(\text{NH}_4)_2[\text{Ce}(\text{NO}_3)_6]$ in a small amount of acetone was added dropwise to the stirring solution of $[\text{CoCp}^*_2][\mathbf{1b}]$. After the color of the solution changed from deep green to bluish dark yellow, the solution was evaporated and well dried in vacuo. To the resulting solid, dichloromethane was added until a total volume of the mixture was 5 mL. The mixture was filtered to remove an insoluble pale ochre solid, and then 0.970 mL of the bluish dark yellow filtrate was diluted with dichloromethane until a total volume of 10 mL. This solution was measured with UV-vis-NIR spectroscopy.

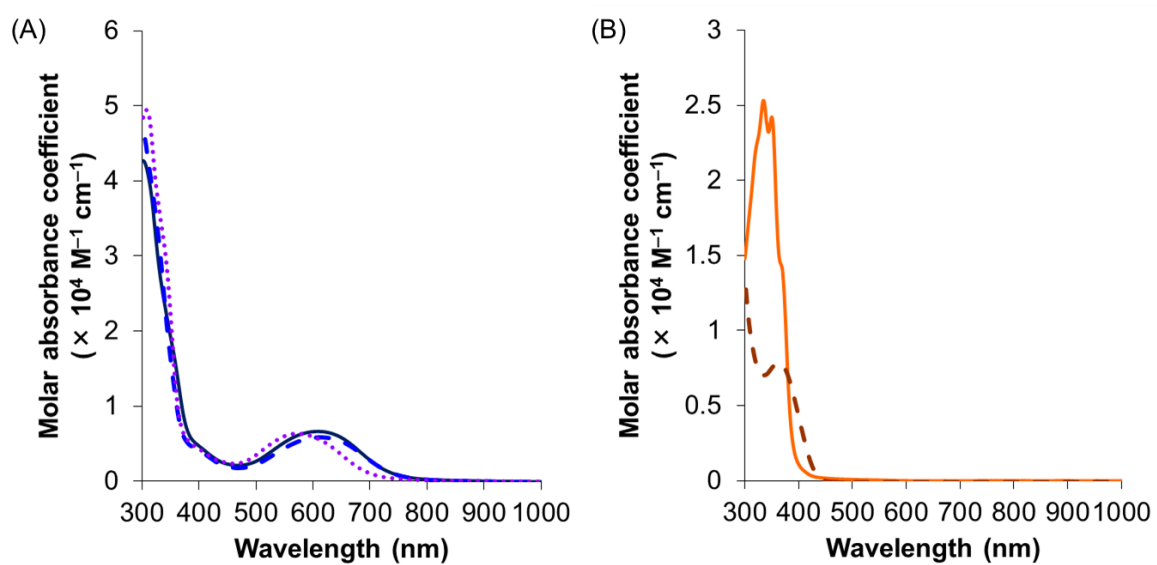


Fig. S1 UV-vis-NIR spectra of **1a** (A, dark blue solid line), **2a** (A, blue dashed line), **3a** (A, violet dotted line), **[4](ClO₄)₂** (B, brown dashed line) and **[5](ClO₄)₂** (B, orange solid line) in DMF.

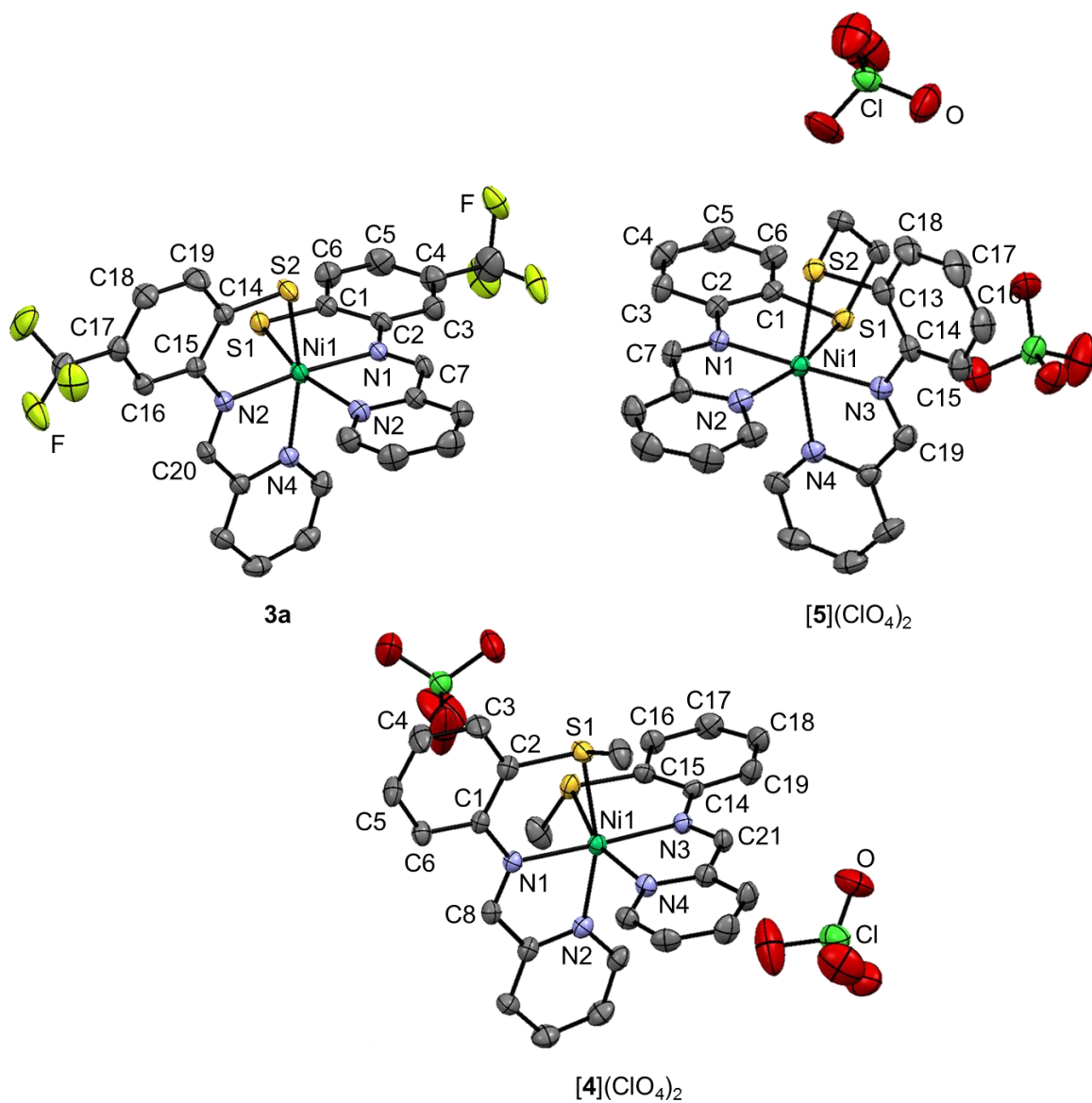


Fig. S2 Structures of **3a** (left), **[4](ClO₄)₂** (center) and **[5](ClO₄)₂** (right). Atoms are drawn as 50% probability thermal ellipsoids. Disordered parts, solvated molecules, and hydrogen atoms are omitted for clarity.

Table S1 Crystal Data and Structure Refinements for 1a, 2a, 3a, [4](ClO₄)₂, [5](ClO₄)₂, [CoCp*₂][1b] and [CoCp*₂][2b]

	1a·DMF	2a	3a	[4](ClO ₄) ₂	[5](ClO ₄) ₂	[CoCp* ₂][1b]·2CH ₂ Cl ₂	[CoCp* ₂][2b]·2CH ₂ Cl ₂	
Empirical formula	C ₂₇ H ₂₅ N ₄ NIOS ₂	C ₃₄ H ₁₆ Cl ₂ N ₄ NI ₂ S ₂	C ₂₉ H ₂₂ FeN ₄ NIOS ₂	C ₃₆ H ₂₄ Cl ₂ N ₄ NIOS ₂	C ₃₀ H ₂₈ Cl ₂ N ₆ NIOS ₂	C ₄₆ H ₅₂ Cl ₄ CoN ₄ NI ₂ S ₂	C ₄₆ H ₅₀ Cl ₆ CoN ₄ NI ₂ S ₂	
Formula weight	558.35	554.14	679.33	714.22	794.31	984.51	1053.40	
Temperature	200 K	200 K	200 K	200 K	200 K	200 K	200 K	
Crystal color, morphology	black, block	black, block	black, plate	brown, needle	orange, block	black, plate	green, plate	
Crystal size	0.11 × 0.10 × 0.04 mm ³	0.21 × 0.14 × 0.10 mm ³	0.28 × 0.22 × 0.08 mm ³	0.07 × 0.05 × 0.04 mm ³	0.16 × 0.15 × 0.08 mm ³	0.55 × 0.17 × 0.07 mm ³	0.55 × 0.42 × 0.06 mm ³	
Crystal system	monoclinic	triclinic	triclinic	orthorhombic	monoclinic	monoclinic	triclinic	
Space group	<i>P</i> 2 ₁ / <i>c</i>	<i>P</i> $\bar{1}$	<i>P</i> $\bar{1}$	<i>P</i> 2 ₁ 2 ₁ 2 ₁	<i>Cc</i>	<i>P</i> 2 ₁ / <i>n</i>	<i>P</i> $\bar{1}$	
Unit cell dimensions	<i>a</i> = 11.3962(4) Å <i>b</i> = 18.9231(4) Å <i>c</i> = 12.9723(4) Å β = 114.313(4) °	<i>a</i> = 8.9125(3) Å <i>b</i> = 12.1348(5) Å <i>c</i> = 12.2295(5) Å α = 67.774(4) ° β = 69.928(3) ° γ = 87.213(3) °	<i>a</i> = 10.3997(2) Å <i>b</i> = 12.7078(2) Å <i>c</i> = 13.3086(3) Å α = 114.490(2) ° β = 111.726(2) ° γ = 92.4482(17) °	<i>a</i> = 8.5516(3) Å <i>b</i> = 10.2011(3) Å <i>c</i> = 33.0145(8) Å	<i>a</i> = 21.948(2) Å <i>b</i> = 8.33062(19) Å <i>c</i> = 20.7006(8) Å β = 115.404(5) °	<i>a</i> = 12.3345(4) Å <i>b</i> = 22.2711(6) Å <i>c</i> = 18.1248(7) Å β = 109.540(4) °	<i>a</i> = 10.1761(3) Å <i>b</i> = 12.4123(4) Å <i>c</i> = 19.1814(5) Å α = 96.674(2) ° β = 91.868(2) ° γ = 96.713(3) °	
Volume	2549.38(15) Å ³	1144.97(9) Å ³	1446.31(6) Å ³	2880.04(15) Å ³	3419.0(4) Å ³	4692.2(3) Å ³	2387.24(12) Å ³	
<i>Z</i>	4	2	2	4	4	4	2	
Density (calculated)	1.455 g/cm ³	1.607 g/cm ³	1.560 g/cm ³	1.647 g/cm ³	1.543 g/cm ³	1.394 g/cm ³	1.465 g/cm ³	
<i>R</i> ₁ (<i>I</i> > 2.00σ(<i>I</i>)) ^a	0.0446	0.0348	0.0310	0.0505	0.0346	0.0767	0.0481	
<i>wR</i> ₂ (all reflections) ^b	0.1220	0.0917	0.0880	0.1271	0.0941	0.2248	0.1300	
Goodness of fit indicator	1.065	1.047	1.059	1.043	1.060	1.043	1.030	

a) $R_1 = \frac{\sum ||F_o| - |F_c||}{\sum |F_o|}$

b) $wR_2 = \left[\frac{\sum (w(F_o^2 - F_c^2))^2}{\sum w(F_o^2)} \right]^{1/2}$

Table S2 Selected Bond Lengths (Å) and Dihedral Angles (deg) for 1a, 2a, 3a, [4]²⁺, [5]²⁺, [1b]⁻ and [2b]⁻

	1a	2a	3a	[4]²⁺	[5]²⁺	[1b]⁻	[2b]⁻
Ni(1)-S(1)	2.4035(11)	2.3780(9)	2.3961(6)	2.4543(14)	2.4033(8)	2.1467(15)	2.1474(9)
Ni(1)-S(2)	2.3833(8)	2.3790(8)	2.393(7)	2.4220(14)	2.4086(11)	2.1531(13)	2.1334(8)
Ni(1)-N(1)	2.037(2)	2.032(2)	2.0420(19)	2.029(4)	2.032(2)	1.834(4)	1.823(2)
Ni(1)-N(3)	2.037(2)	2.030(2)	2.0476(19)	2.045(4)	2.032(2)	1.829(4)	1.828(2)
Ni(1)-N(2)	2.142(3)	2.157(2)	2.1342(15)	2.088(4)	2.068(3)		
Ni(1)-N(4)	2.127(2)	2.129(2)	2.137(2)	2.077(4)	2.061(4)		
S(1)-C(1)	1.747(3)	1.742(3)	1.736(2)	1.779(5)	1.788(3)	1.751(5)	1.743(3)
S(2)-C(13)	1.737(3)	1.735(3)	1.734(3)	1.779(5)	1.781(3)	1.738(5)	1.744(3)
N(1)-C(2)	1.418(4)	1.405(4)	1.417(3)	1.405(6)	1.410(4)	1.352(7)	1.359(3)
N(3)-C(14)	1.409(4)	1.410(3)	1.416(3)	1.407(6)	1.427(5)	1.366(6)	1.355(3)
N(1)-C(7)	1.281(5)	1.282(3)	1.283(2)	1.285(6)	1.286(4)	1.464(7)	1.465(4)
N(3)-C(19)	1.285(3)	1.281(4)	1.285(3)	1.282(6)	1.280(5)	1.453(6)	1.451(3)
C(1)-C(2)	1.402(5)	1.404(3)	1.417(3)	1.405(7)	1.392(4)	1.413(8)	1.428(5)
C(13)-C(14)	1.409(4)	1.406(4)	1.415(4)	1.394(7)	1.396(6)	1.422(6)	1.426(4)
C(1)-C(6)	1.409(5)	1.405(5)	1.411(3)	1.387(7)	1.394(5)	1.419(8)	1.392(5)
C(13)-C(18)	1.407(4)	1.405(4)	1.410(3)	1.399(7)	1.395(6)	1.416(7)	1.392(4)
C(2)-C(3)	1.396(4)	1.399(4)	1.393(3)	1.404(6)	1.402(4)	1.421(7)	1.400(4)
C(14)-C(15)	1.396(4)	1.393(3)	1.394(3)	1.401(7)	1.401(4)	1.415(7)	1.396(4)
C(3)-C(4)	1.369(6)	1.365(5)	1.380(3)	1.376(7)	1.381(5)	1.371(10)	1.373(4)
C(15)-C(16)	1.370(5)	1.369(4)	1.380(3)	1.382(8)	1.365(7)	1.375(8)	1.382(4)
C(4)-C(5)	1.383(6)	1.373(4)	1.398(3)	1.376(8)	1.374(5)	1.398(10)	1.364(6)
C(16)-C(17)	1.380(4)	1.382(4)	1.397(4)	1.390(8)	1.377(8)	1.397(8)	1.387(6)
C(5)-C(6)	1.376(5)	1.371(4)	1.370(4)	1.383(8)	1.389(4)	1.373(9)	1.382(6)
C(17)-C(18)	1.381(5)	1.365(4)	1.364(4)	1.372(8)	1.377(5)	1.361(8)	1.355(6)
Dihedral angle ^a	83.51	84.47	86.76	85.77	87.95	1.27	4.34

^aDihedral angle composed of NiSN planes

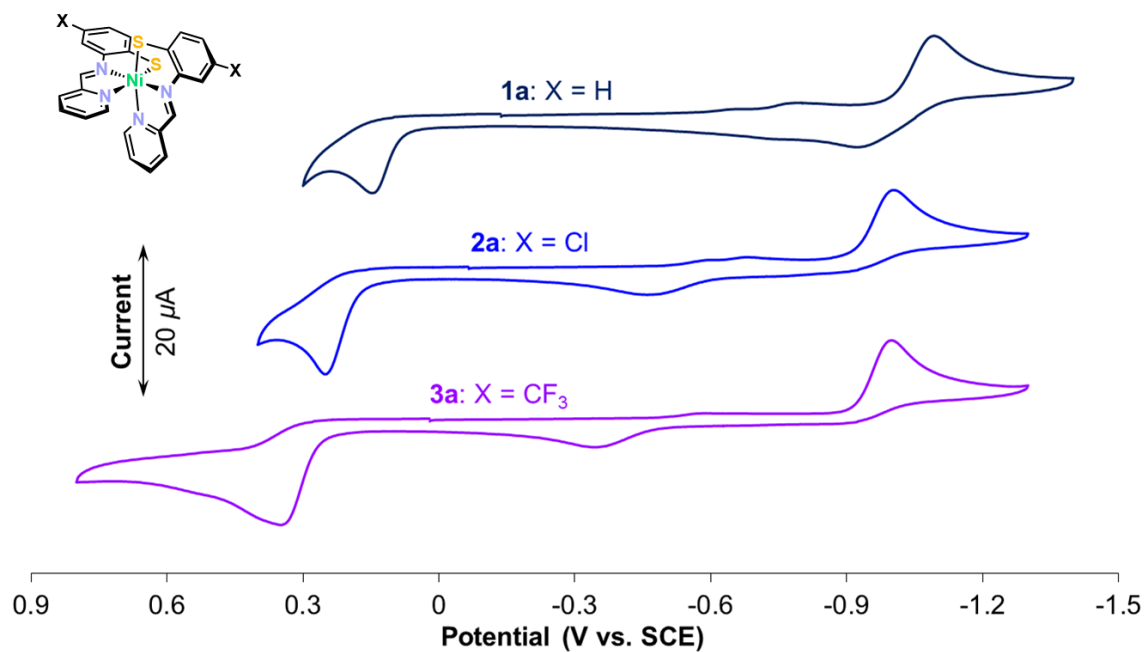


Fig. S3 Cyclic voltammograms of 1.0 mM **1a** (top dark blue line), **2a** (middle blue line) and **3a** (bottom violet line) in DMF containing 0.10 M ^tBu₄NClO₄ as electrolyte using a glassy carbon working electrode, a platinum wire auxiliary electrode and a saturated calomel reference electrode at a scan rate of 50 mV/s.

Table S3 Oxidation and Reduction Potentials of **1a**, **2a** and **3a**

		E_1	E_2	E_4
1a	Red			-1.09
	Ox	0.15		-0.92
	Redox			-1.01 qr
2a	Red			-1.00
	Ox	0.25	-0.46	
3a	Red			-1.00
	Ox	0.35	-0.34	

Potential/V vs. SCE. qr: Quasi-reversible.

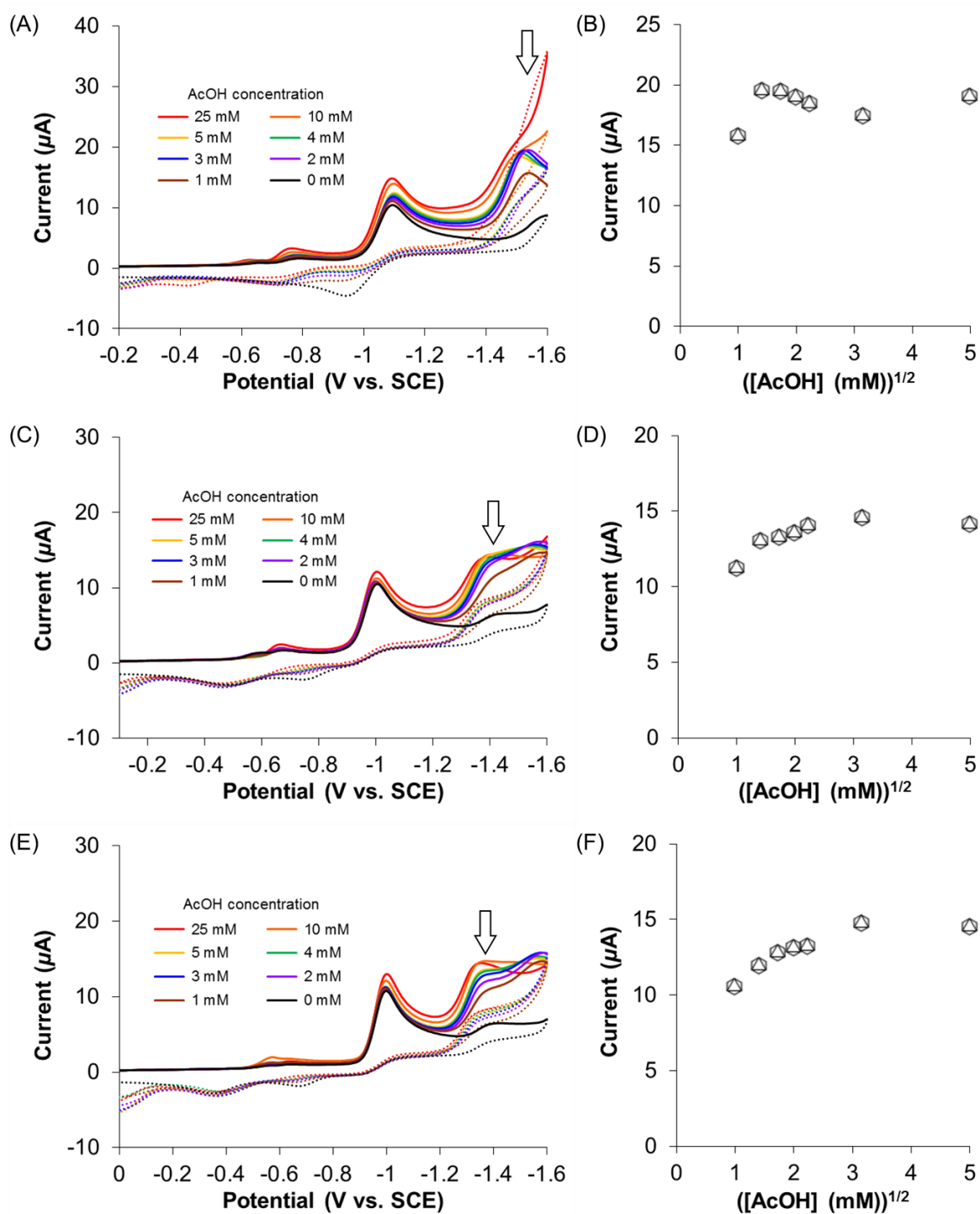


Fig. S4 Cyclic voltammograms of 1.0 mM (A) **1a**, (C) **2a** and (E) **3a** in DMF containing 0.10 M $n\text{Bu}_4\text{NClO}_4$ as electrolyte in the presence of various concentrations of AcOH using a glassy carbon working electrode, a platinum wire auxiliary electrode and a saturated calomel reference electrode at a scan rate of 50 mV/s. Return traces are indicated by dotted lines. Plots of peak currents for new reduction waves (hollow arrow) of (B) **1a**, (D) **2a** and (F) **3a** observed after addition of AcOH vs. $([\text{AcOH}] \text{ (mM)})^{1/2}$.

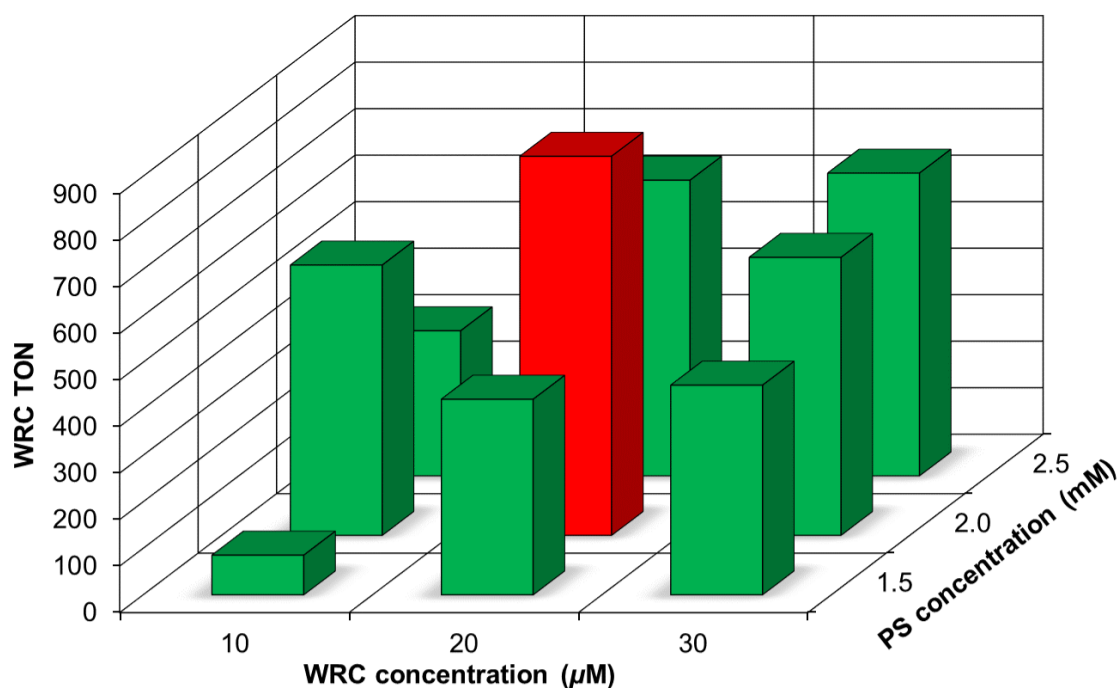


Fig. S5 (A) Performances of **1a** as a WRC in a photocatalytic hydrogen evolution system containing various concentration of WRC and PS ($[\text{Ir}(\text{ppy})_2(\text{bpy})]\text{PF}_6$) under 5 vol. % SED (TEOA) and 15 vol. % H_2O in DMF upon irradiation with 500 W xenon lamp ($\lambda > 400 \text{ nm}$) at r.t. and 308.7 ± 4.7 Torr initial pressure.

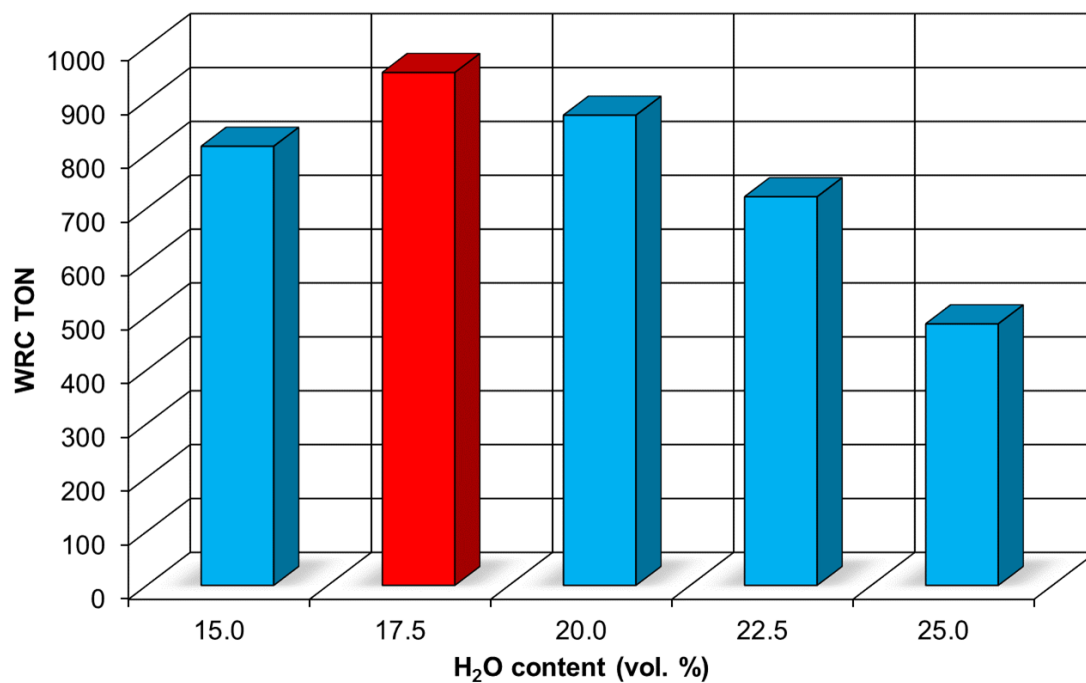


Fig. S5 (B) Performances of **1a** as a WRC in a photocatalytic hydrogen evolution system containing 20 μM WRC, 2.0 mM PS ($[\text{Ir}(\text{ppy})_2(\text{bpy})]\text{PF}_6$), 5 vol. % SED (TEOA) and various content (vol. %) of H_2O in DMF upon irradiation with 500 W xenon lamp ($\lambda > 400 \text{ nm}$) at r.t. and 309.1 ± 8.5 Torr initial pressure.

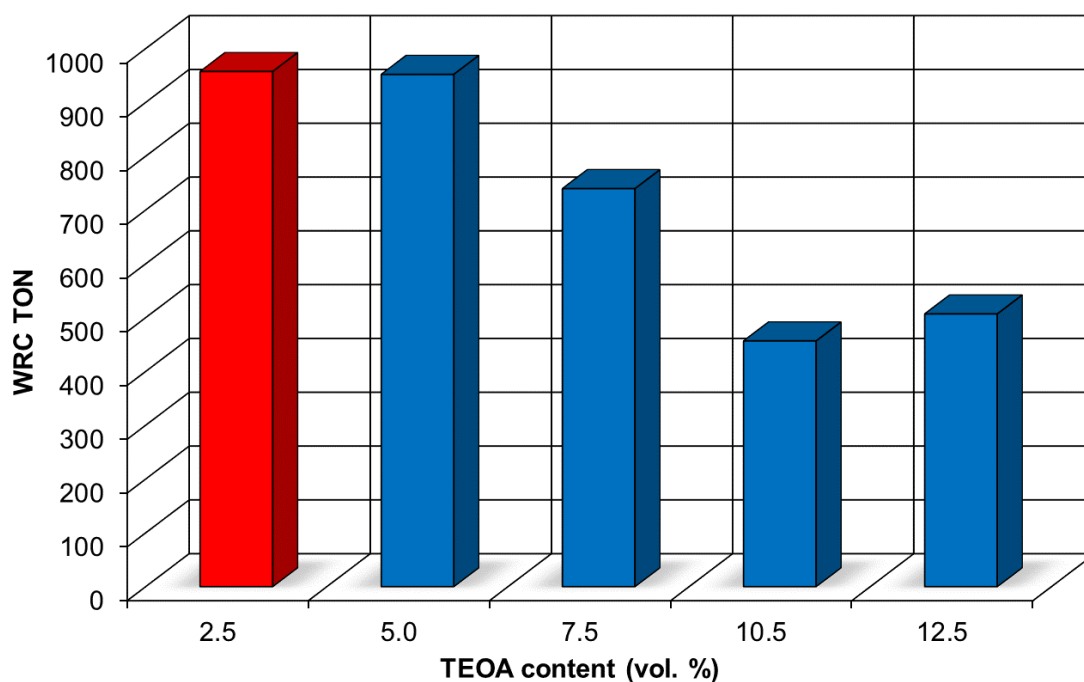


Fig. S5 (C) Performances of **1a** as a WRC in a photocatalytic hydrogen evolution system containing 20 μM WRC, 2.0 mM PS ($[\text{Ir}(\text{ppy})_2(\text{bpy})]\text{PF}_6$), various content (vol. %) of SED (TEOA) and 17.5 vol. % H_2O in DMF upon irradiation with 500 W xenon lamp ($\lambda > 400 \text{ nm}$) at r.t. and 310.1 ± 8.3 Torr initial pressure.

Table S4 Performances of **1a** as a WRC under Various Conditions

[WRC] (μM)	[PS] (mM)	SED content (vol. %)	H_2O content (vol. %)	H_2 evolution (μmol)	WRC TON	WRC TOF _{max} (h^{-1})	Conversion (%)
10	1.5	5.0	15.0	8.6	85	12 (2 h)	0.010
10	2.0	5.0	15.0	56.3	581	24 (24 h)	0.068
10	2.5	5.0	15.0	30.2	312	26 (6 h)	0.036
20	1.5	5.0	15.0	83.2	420	30 (7 h)	0.100
20	2.0	5.0	15.0	161.2	815	53 (5 h)	0.194
20	2.5	5.0	15.0	129.7	636	37 (7 h)	0.156
30	1.5	5.0	15.0	135.6	451	23 (8 h)	0.163
30	2.0	5.0	15.0	177.4	598	35 (6 h)	0.214
30	2.5	5.0	15.0	198.5	651	48 (4 h)	0.239
20	2.0	5.0	17.5	192.3	952	46 (9 h)	0.198
20	2.0	5.0	20.0	176.3	873	51 (5 h)	0.159
20	2.0	5.0	22.5	142.7	721	56 (4 h)	0.115
20	2.0	5.0	25.0	98.0	485	35 (5 h)	0.071
20	2.0	2.5	17.5	187.4	957	48 (7 h)	0.193
20	2.0	7.5	17.5	146.3	740	42 (8 h)	0.151
20	2.0	10.5	17.5	91.3	456	21 (12 h)	0.094
20	2.0	12.5	17.5	99.2	507	39 (5 h)	0.102

In a photocatalytic hydrogen evolution system containing WRC (**1a**), PS ($[\text{Ir}(\text{ppy})_2(\text{bpy})]\text{PF}_6$), SED (TEOA) and H_2O in DMF upon irradiation with 500 W xenon lamp ($\lambda > 400 \text{ nm}$) at r.t. and 309.5 ± 8.9 Torr initial pressure. **Red bold letters**: Optimum condition.

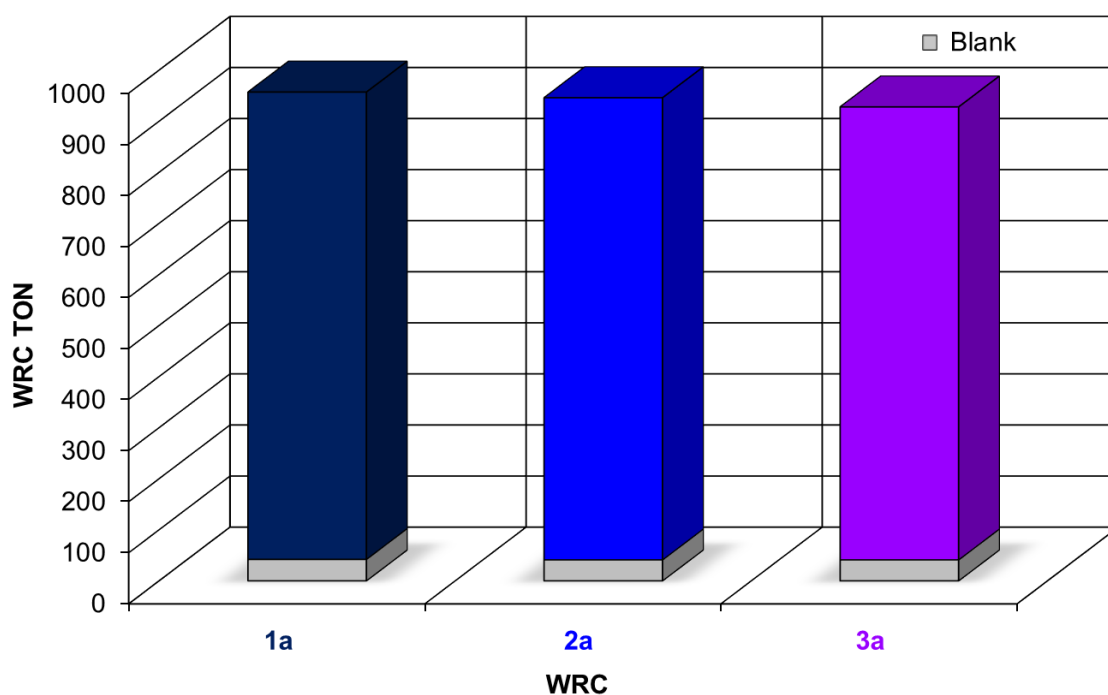


Fig. S6 Performances of **1a**, **2a** and **3a** as WRCs in a photocatalytic hydrogen evolution system containing 20 μM WRC, 2.0 mM PS ($[\text{Ir}(\text{ppy})_2(\text{bpy})]\text{PF}_6$), 2.5 vol. % SED (TEOA) and 17.5 vol. % H_2O in DMF upon irradiation with 500 W xenon lamp ($\lambda > 400 \text{ nm}$) at r.t. and 310.3 ± 9.0 Torr initial pressure.

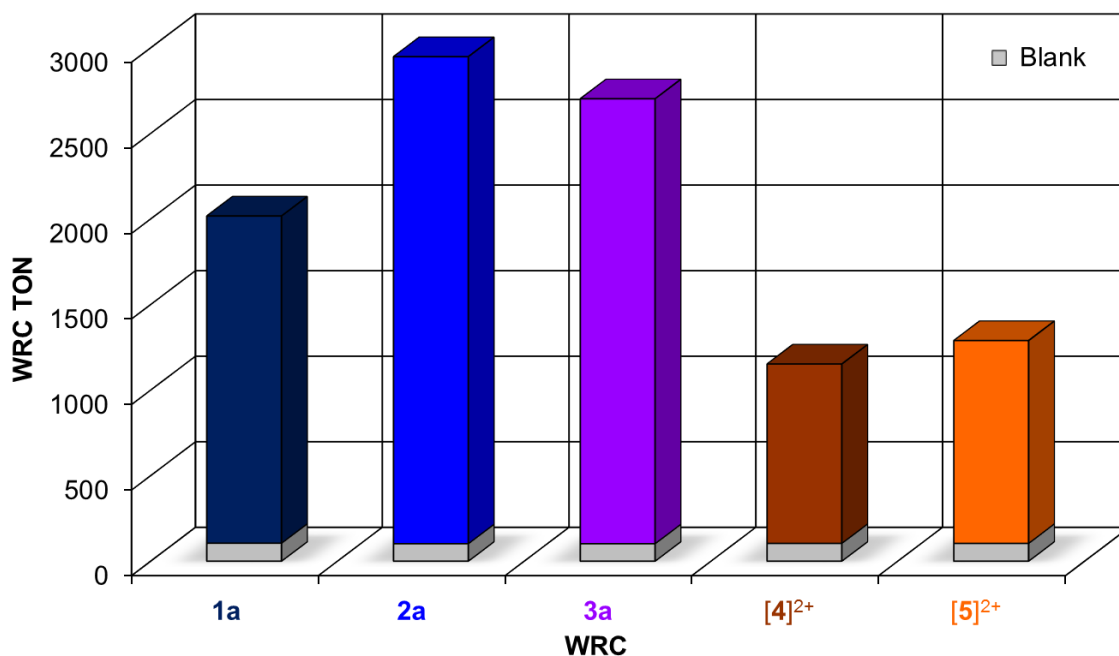


Fig. S7 Performances of **1a**, **2a**, **3a**, **[4]**(ClO_4)₂ and **[5]**(ClO_4)₂ as WRCs in a photocatalytic hydrogen evolution system containing 20 μM WRC, 2.0 mM PS ($[\text{Ir}(\text{ppy})_2(\text{bpy})]\text{PF}_6$), 2.5 vol. % SED (TEA) and 17.5 vol. % H_2O in DMF upon irradiation with 500 W xenon lamp ($\lambda > 400 \text{ nm}$) at r.t. and 318.8 ± 6.4 Torr initial pressure.

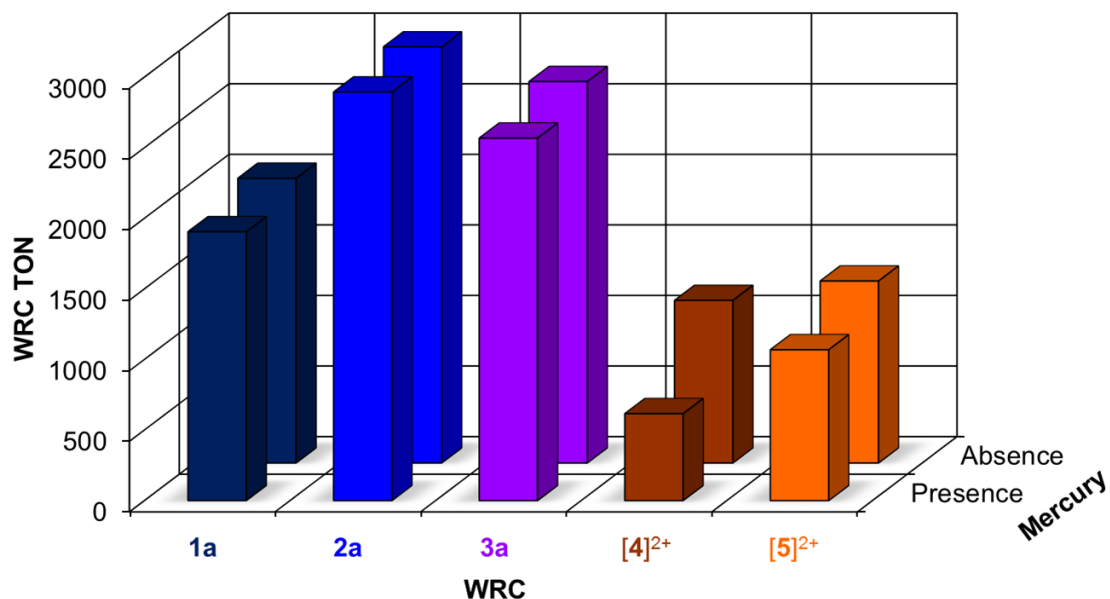


Fig. S8 Performances of **1a**, **2a**, **3a**, **[4](ClO₄)₂** and **[5](ClO₄)₂** as WRCs in a photocatalytic hydrogen evolution system containing 20 μ M WRC, 2.0 mM PS ([Ir(ppy)₂(bpy)]PF₆), 2.5 vol. % SED (TEA), and 17.5 vol. % H₂O in DMF in the presence or absence of ca. 1600 equiv. (relative to WRC) of Hg upon irradiation with 500 W xenon lamp ($\lambda > 400$ nm) at r.t. and 313.7 \pm 11.5 Torr initial pressure.

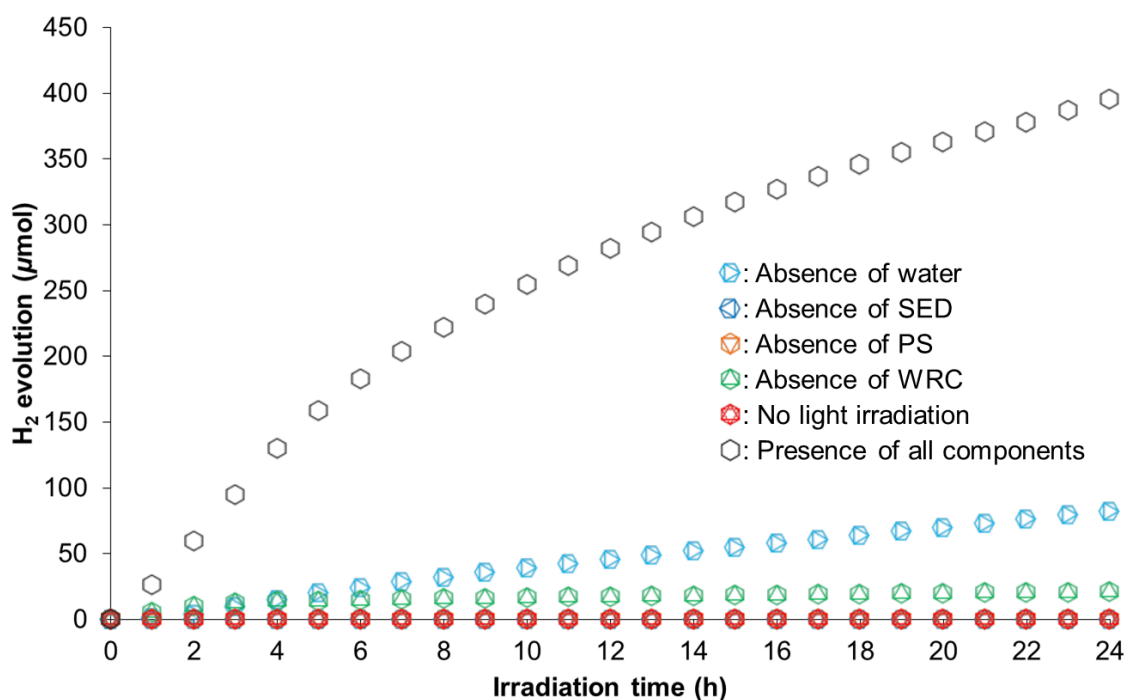


Fig. S9 Hydrogen evolution in a photocatalytic system in the absence of any components of 20 μ M WRC (**1a**), 2.0 mM PS ([Ir(ppy)₂(bpy)]PF₆), 2.5 vol. % SED (TEA) and 17.5 vol. % H₂O in DMF upon irradiation with 500 W xenon lamp ($\lambda > 400$ nm) at r.t. and 322.9 \pm 12.5 Torr initial pressure.

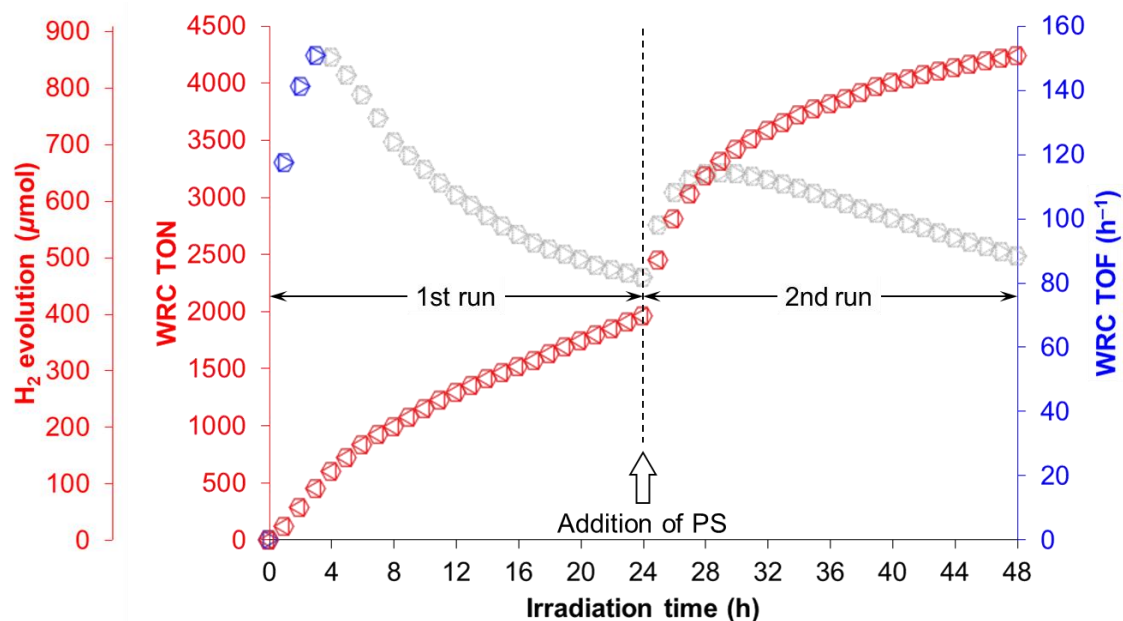


Fig. S10 Performance of **1a** as a WRC in a photocatalytic hydrogen evolution system containing 20 μM WRC, 2.0 mM (0–24 h, 1st run) or 4.0 mM (24–48 h, 2nd run) PS ($[\text{Ir}(\text{ppy})_2(\text{bpy})]\text{PF}_6$), 2.5 vol. % SED (TEA) and 17.5 vol. % H_2O in DMF upon irradiation with 500 W xenon lamp ($\lambda > 400 \text{ nm}$) at r.t. and 319.2 \pm 6.9 Torr initial pressure. After the final quantitation of H_2 in the 1st run (0–24 h), the same amount of PS as the initial condition was added to the system (hollow arrow).

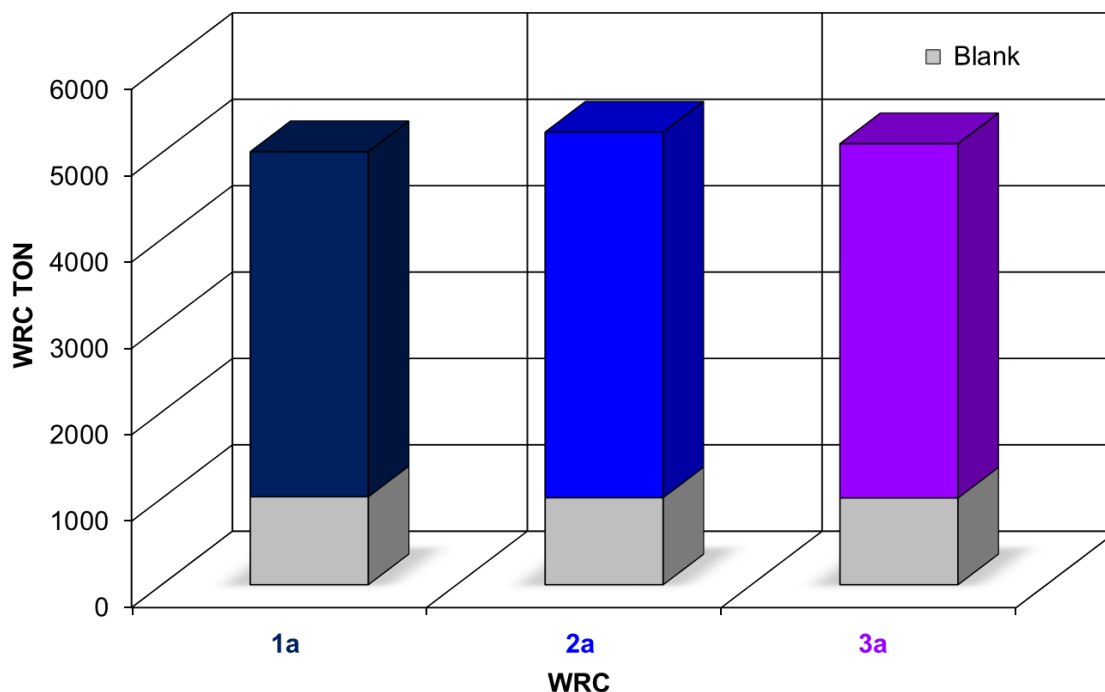


Fig. S11 Performances of **1a**, **2a**, and **3a** as WRCs in a photocatalytic hydrogen evolution system containing 20 μM WRC, 2.0 mM PS ($[\text{Ir}(\text{dtbppy})_2(\text{bpy})]\text{PF}_6$), 2.5 vol. % SED (TEA) and 17.5 vol. % H_2O in DMF upon irradiation with 500 W xenon lamp ($\lambda > 400 \text{ nm}$) at r.t. and 314.1 \pm 1.1 Torr initial pressure.

Table S5 Performances of 1a, 2a, 3a, [4]²⁺ and [5]²⁺ as WRCs

PS	SED	WRC	H ₂ evolution (μmol)	WRC TON	WRC TOF _{max} (h ⁻¹)	Conversion (%)
[Ir(ppy) ₂ (bpy)] ⁺	TEOA	1a	187	957	48 (7 h)	0.19
		2a	191	946	50 (7 h)	0.20
		3a	187	928	43 (11 h)	0.19
			8.3			0.0086
[Ir(ppy) ₂ (bpy)] ⁺	TEA	1a	395	2017	165 (4 h)	0.41
		2a	594	2948	330 (2 h)	0.61
		3a	542	2702	234 (3 h)	0.56
		[4] ²⁺	227	1152	73 (5 h)	0.23
		[5] ²⁺	254	1289	174 (1 h)	0.26
		21			0.021	
[Ir(ppy) ₂ (dtbbpy)] ⁺	TEA	1a	1002	5012	1072 (2 h)	1.0
		2a	1059	5239	1089 (2 h)	1.1
		3a	1035	5104	932 (2 h)	1.1
			204			0.21

In a photocatalytic hydrogen evolution system containing 20 μM WRC (**1a**, **2a**, **3a**, [4](ClO₄)₂ or [5](ClO₄)₂), 2.0 mM PS ([Ir(ppy)₂(bpy)]PF₆ or [Ir(ppy)₂(dtbbpy)]PF₆), 2.5 vol. % SED (TEOA or TEA) and 17.5 vol. % H₂O in DMF upon irradiation with 500 W xenon lamp (λ > 400 nm) at r.t. and 313.3 ± 12.0 Torr initial pressure.

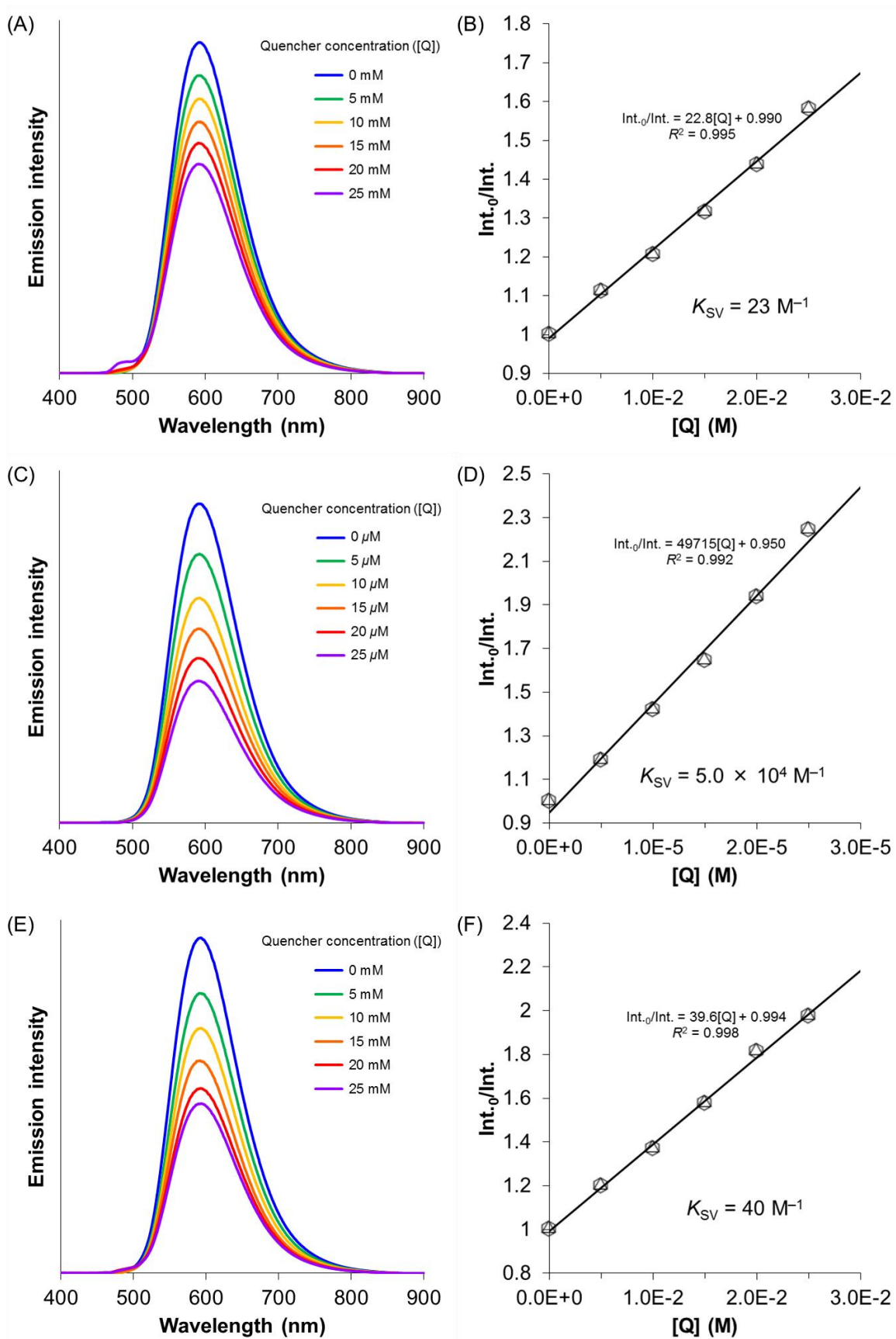


Fig. S12 Emission spectra of 0.20 mM $[\text{Ir}(\text{ppy})_2(\text{bpy})]\text{PF}_6$ excited at 337 nm in DMF in the presence of various concentrations of (A) TEOA, (C) **1a** and (E) TEA. Stern-Volmer plots of emission intensity at 593 nm using (B) TEOA, (D) **1a** and (F) TEA as a quencher.

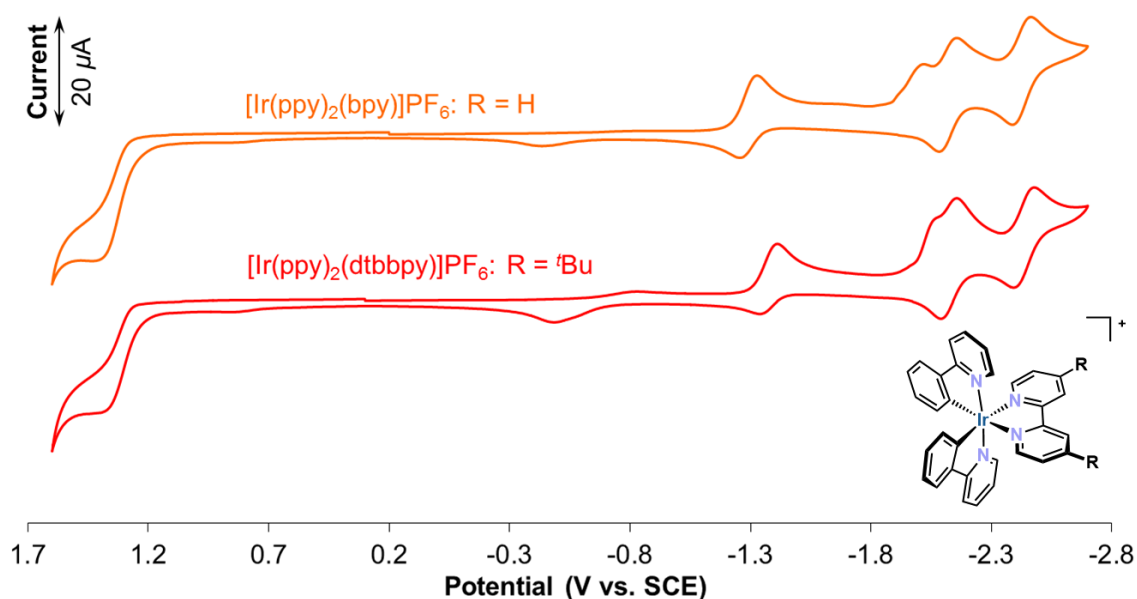


Fig. S13 Cyclic voltammograms of 1.0 mM $[\text{Ir}(\text{ppy})_2(\text{bpy})]\text{PF}_6$ (top orange line) and $[\text{Ir}(\text{ppy})_2(\text{dtbbpy})]\text{PF}_6$ (bottom red line) in DMF containing 0.10 M $n\text{Bu}_4\text{NClO}_4$ as electrolyte using a glassy carbon working electrode, a platinum wire auxiliary electrode and a saturated calomel reference electrode at a scan rate of 50 mV/s.

Table S6 Oxidation and Reduction Potentials of $[\text{Ir}(\text{ppy})_2(\text{bpy})]^+$ and $[\text{Ir}(\text{ppy})_2(\text{dtbbpy})]^+$

$[\text{Ir}(\text{ppy})_2\text{L}]^+$		E_1 ($\text{Ir}^{\text{III/IV}}$)	E_2 ($\text{L}^{0/1-}$)	E_3	E_4	E_5	$*E_{\text{ox}}$	$*E_{\text{red}}$
$[\text{Ir}(\text{ppy})_2(\text{dtbbpy})]^+$ (L = dtbbpy: R = $t\text{Bu}$)	Red		-1.41	-2.06	-2.16	-2.48		0.74
	Ox	1.37	-1.34		-2.09	-2.39	-0.78	
	Redox		-1.37 r		-2.12 r	-2.44 qr		
$[\text{Ir}(\text{ppy})_2(\text{bpy})]^+$ (L = bpy: R = H)	Red		-1.33	-2.02	-2.16	-2.46		0.76
	Ox	1.43	-1.26		-2.08	-2.39	-0.66	
	Redox		-1.29 r		-2.12 r	-2.43 qr		

Potential/V vs. SCE. r: reversible; qr: Quasi-reversible. $*E_{\text{ox}}$, $*E_{\text{red}}$: excited state oxidation and reduction potentials calculated using Hess's law on the basis of recorded potentials and emission energy⁹, $E_{\lambda\text{em}}$; $*E_{\text{ox}} = E_{\text{ox}} - E_{\lambda\text{em}}$, $*E_{\text{red}} = E_{\text{red}} + E_{\lambda\text{em}}$, $E_{\lambda\text{em}} = 2.15$ and 2.09 eV for $[\text{Ir}(\text{ppy})_2(\text{dtbbpy})]\text{PF}_6$ and $[\text{Ir}(\text{ppy})_2(\text{bpy})]\text{PF}_6$, respectively.

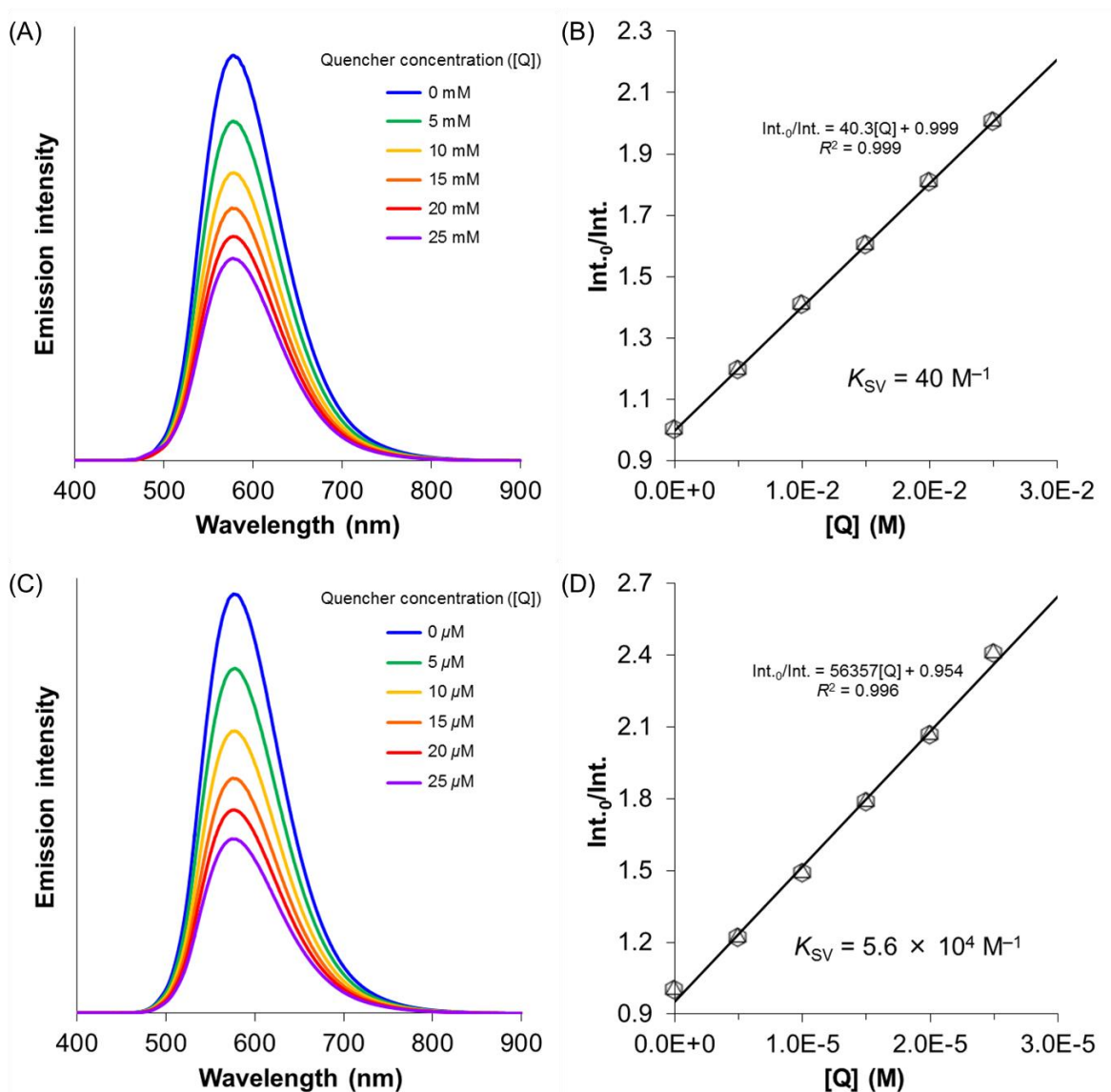


Fig. S14 Emission spectra of 0.20 mM $[\text{Ir}(\text{ppy})_2(\text{dtbbpy})]\text{PF}_6$ excited at 337 nm in DMF in the presence of various concentrations of (A) TEA and (C) **1a**. Stern-Volmer plots of emission intensity at 578 nm using (B) TEA and (D) **1a** as a quencher.

Table S7 Emission Quenching Data Using SED or WRC as a Quencher

Emitter	Quencher	$K_{\text{SV}} (\text{M}^{-1})$	$k_{\text{q}} (= K_{\text{SV}}/\tau)$ ($\text{M}^{-1} \text{s}^{-1}$) ^a	$[\text{Q}] (\text{M})$ ^b	$\nu (= k_{\text{q}}[\text{Q}])$ (s^{-1})
$[\text{Ir}(\text{ppy})_2(\text{dtbbpy})]\text{PF}_6$	TEA	40	7.4×10^7	0.18	1.3×10^7
	1a	5.6×10^4	1.0×10^{11}	20×10^{-6}	2.0×10^6
$[\text{Ir}(\text{ppy})_2(\text{bpy})]\text{PF}_6$	TEOA	23	8.1×10^7	0.18	1.5×10^7
	1a	5.0×10^4	1.8×10^{11}	20×10^{-6}	3.6×10^6

^a $\tau = 0.54 \mu\text{s}$ (for $[\text{Ir}(\text{ppy})_2(\text{dtbbpy})]\text{PF}_6$)¹⁰, $\tau = 285 \text{ ns}$ (for $[\text{Ir}(\text{ppy})_2(\text{bpy})]\text{PF}_6$).¹¹ ^bIn photocatalytic hydrogen evolution system.

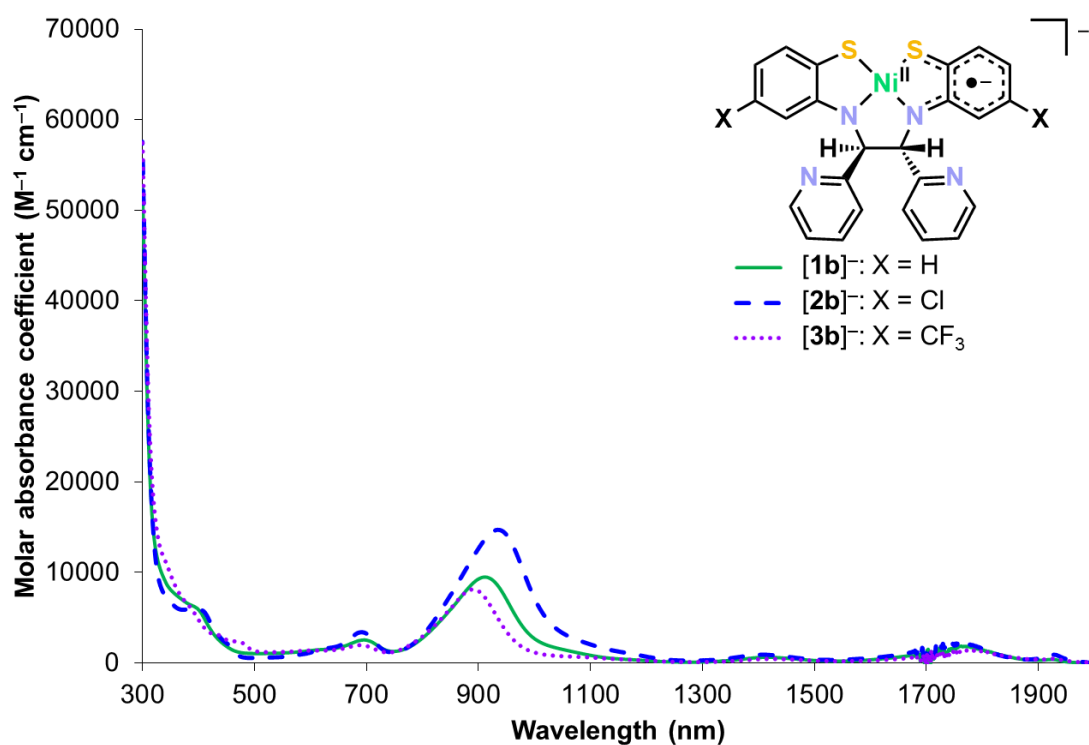


Fig. S15 UV-vis-NIR spectra of [CoCp*₂][**1b**] (green solid line), [CoCp*₂][**2b**] (blue dashed line) and [CoCp*₂][**3b**] (violet dotted line) in DMF.

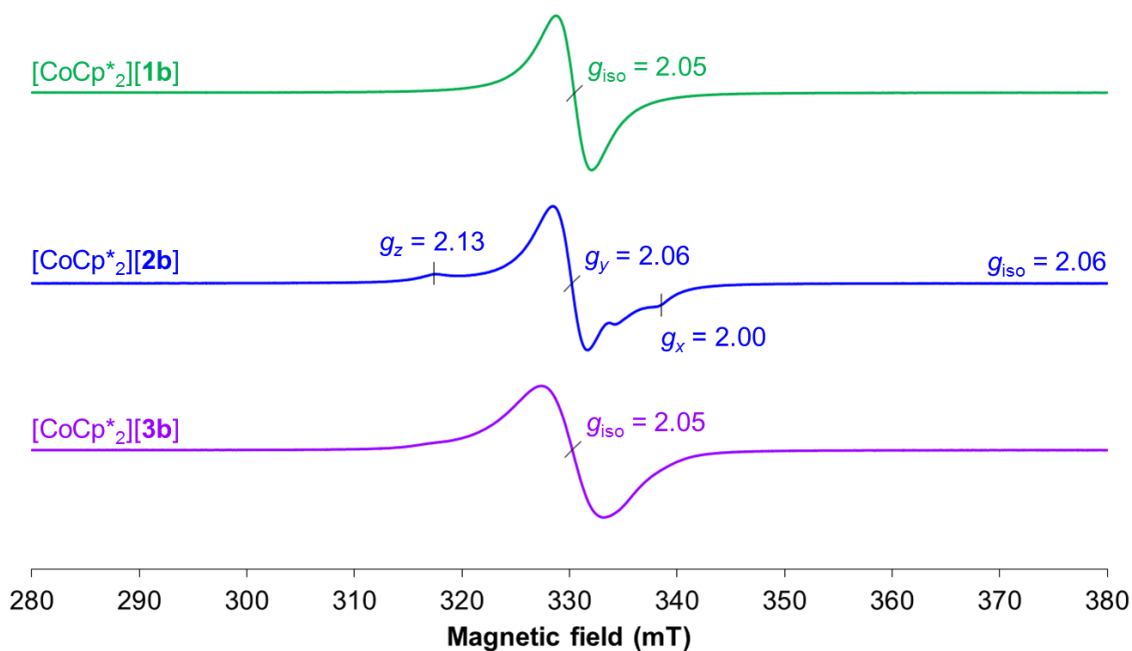


Fig. S16 X-band solid-state ESR spectra of [CoCp*₂][**1b**] (top green line), [CoCp*₂][**2b**] (middle blue line) and [CoCp*₂][**3b**] (bottom violet line) at r.t.. Splitting of central resonance for [CoCp*₂][**2b**] is attributed to hyperfine interaction with one ¹⁴N atom in a N,S-chelating moiety.¹²

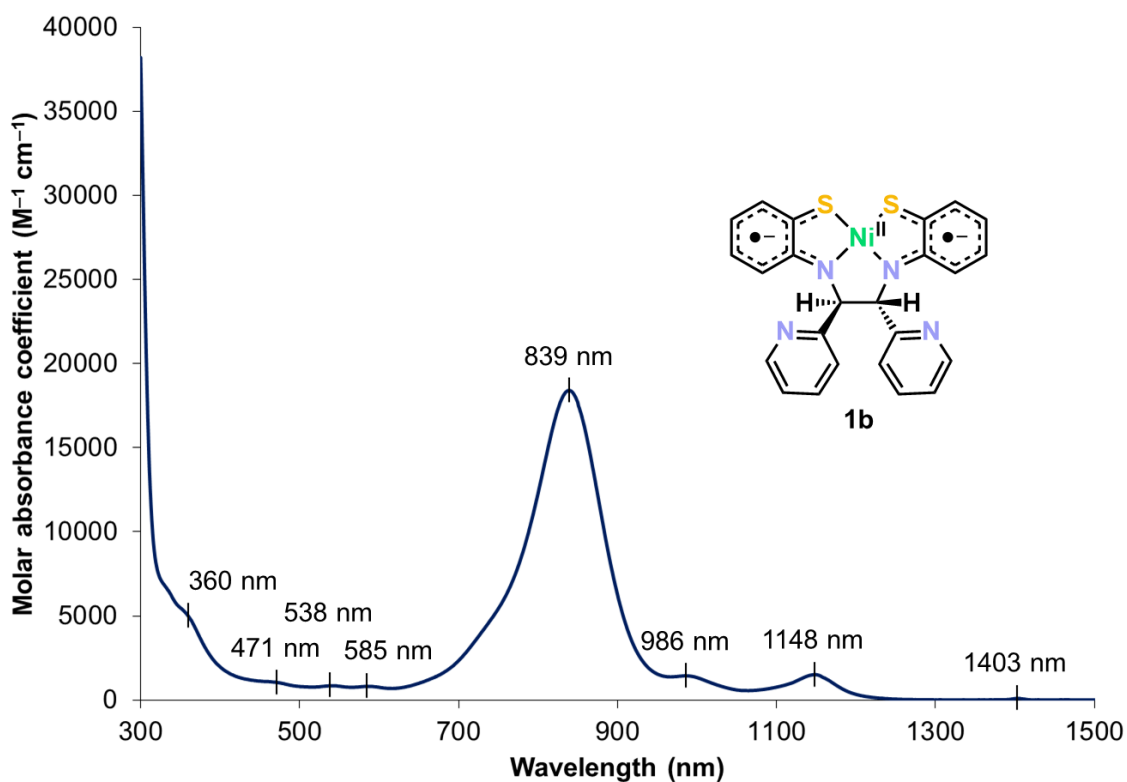


Fig. S17 UV-vis-NIR spectrum of **1b** in CH_2Cl_2 .

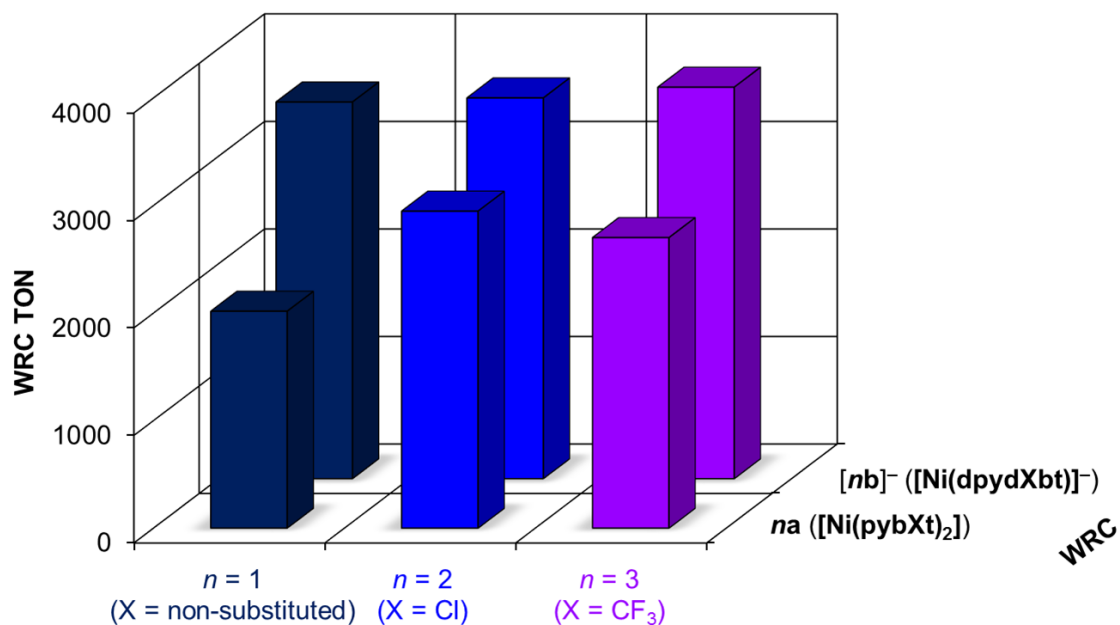


Fig. S18 Performances of **1a**, **2a**, **3a**, $[\text{CoCp}^*_2][\mathbf{1b}]$, $[\text{CoCp}^*_2][\mathbf{2b}]$ and $[\text{CoCp}^*_2][\mathbf{3b}]$ as WRCs in a photocatalytic hydrogen evolution system containing $20 \mu\text{M}$ WRC, 2.0 mM PS ($[\text{Ir}(\text{ppy})_2(\text{bpy})]\text{PF}_6$), $2.5 \text{ vol. } \%$ SED (TEA) and $17.5 \text{ vol. } \%$ H_2O in DMF upon irradiation with 500 W xenon lamp ($\lambda > 400 \text{ nm}$) at r.t. and $312.9 \pm 5.4 \text{ Torr}$ initial pressure.

Table S8 Performances of 1a, 2a, 3a, [1b]⁻, [2b]⁻ and [3b]⁻ as WRCs

WRC	H ₂ evolution (μ mol)	WRC TON	WRC TOF _{max} (h ⁻¹)	Conversion (%)
[1b] ⁻	708	3503	415 (2 h)	0.73
1a	395	2017	165 (4 h)	0.41
[2b] ⁻	721	3541	593 (1 h)	0.74
2a	594	2948	330 (2 h)	0.61
[3b] ⁻	733	3641	591 (2 h)	0.76
3a	542	2702	234 (3 h)	0.56
	21			0.021

In a photocatalytic hydrogen evolution system containing 20 μ M WRC (**1a**, **2a**, **3a**, [CoCp*₂]**1b**), [CoCp*₂]**2b** or [CoCp*₂]**3b**), 2.0 mM PS ([Ir(ppy)₂(bpy)]PF₆), 2.5 vol. % SED (TEA) and 17.5 vol. % H₂O in DMF upon irradiation with 500 W xenon lamp ($\lambda > 400$ nm) at r.t. and 312.9 \pm 5.4 Torr initial pressure.

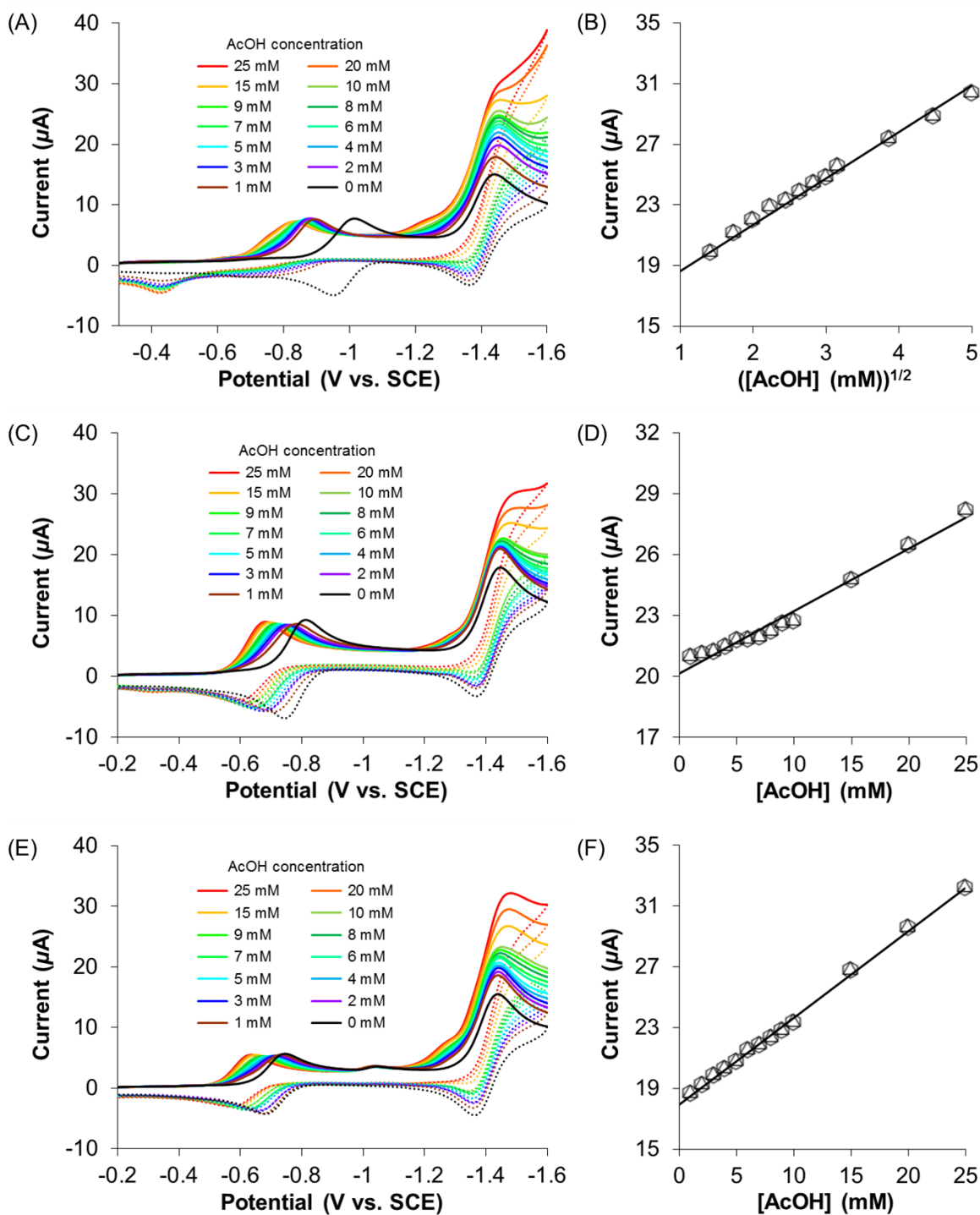


Fig. S19 Cyclic voltammograms of 1.0 mM (A) [CoCp*₂][1b], (C) [CoCp*₂][2b], (E) [CoCp*₂][3b] and (G) [CoCp*₂]PF₆ in DMF containing 0.10 M ⁿBu₄NClO₄ as electrolyte in the presence of various concentrations of AcOH using a glassy carbon working electrode, a platinum wire auxiliary electrode and a saturated calomel reference electrode at a scan rate of 50 mV/s. Return traces are indicated by dotted lines. Plots of *i*_{cat} of (B) [CoCp*₂][1b] vs. (AcOH concentration)^{1/2} and (D) [CoCp*₂][2b] and (F) [CoCp*₂][3b] vs. AcOH concentration. (H) Plots of peak currents for redox wave of [CoCp*₂]⁺⁰ vs. (AcOH concentration)^{1/2}.

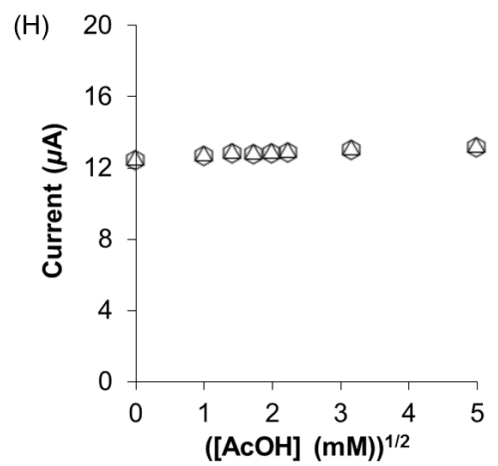
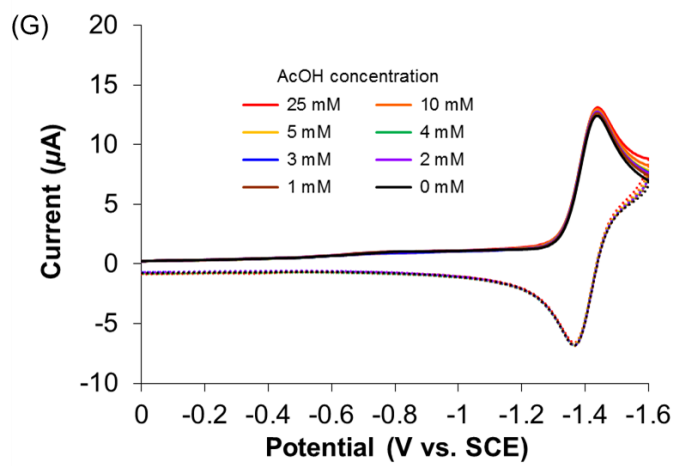


Fig. S19 (Continued)

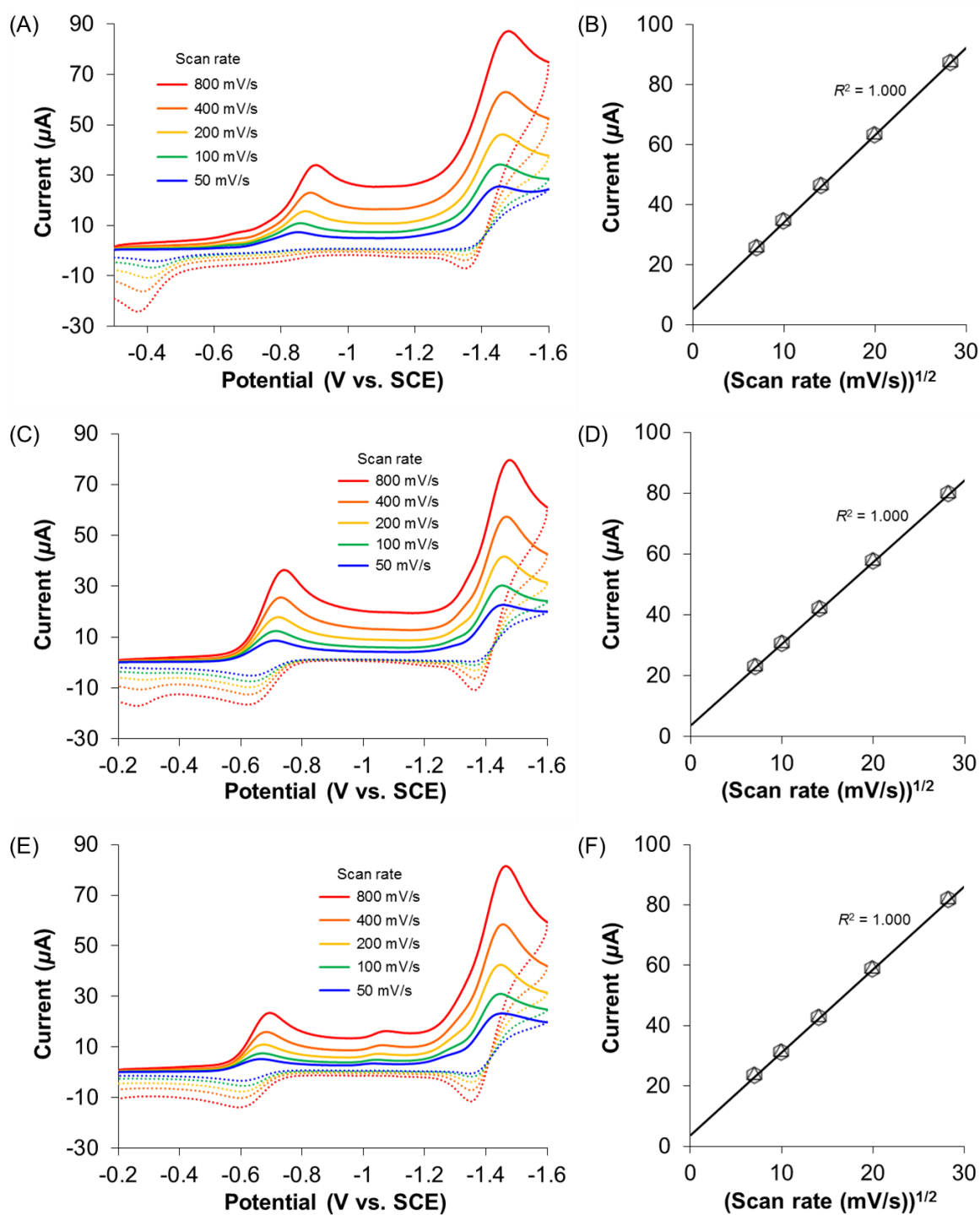


Fig. S20 Cyclic voltammograms of 1.0 mM (A) [CoCp*₂][**1b**], (C) [CoCp*₂][**2b**] and (E) [CoCp*₂][**3b**] in DMF containing 0.10 M ⁿBu₄NClO₄ as electrolyte and 10.0 mM AcOH using a glassy carbon working electrode, a platinum wire auxiliary electrode and a saturated calomel reference electrode at various scan rates. Return traces are indicated by dotted lines. (B, D and F) Plots of *i*_{cat} vs. (scan rate)^{1/2}.

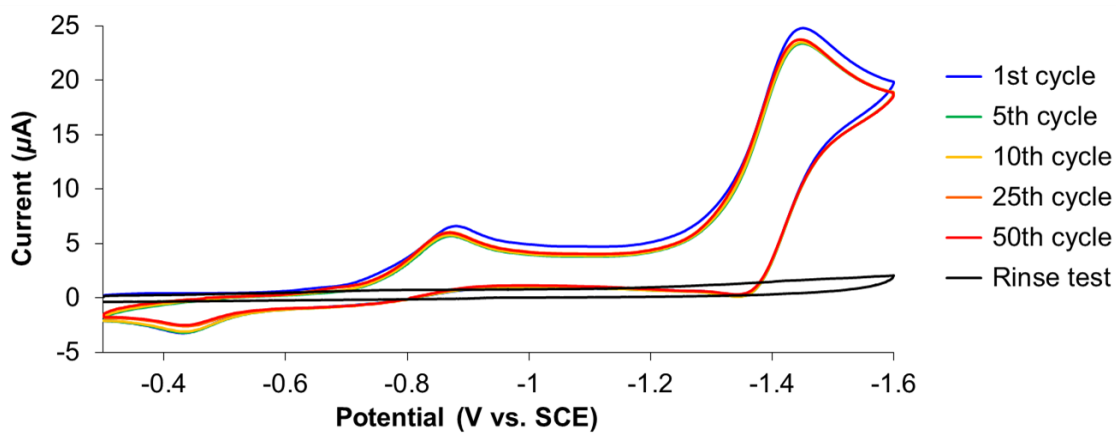


Fig. 21 Cyclic voltammograms of 1.0 mM [CoCp*₂][**1b**] in DMF containing 0.10 M ^tBu₄NClO₄ as electrolyte and 10.0 mM AcOH using a glassy carbon working electrode, a platinum wire auxiliary electrode and a saturated calomel reference electrode at a scan rate of 50 mV/s. The 1st, 5th, 10th, 25th and 50th cycles are only shown for clarity. Black line shows the result of the rinse test, which was recorded using the same solution free of [CoCp*₂][**1b**] after 50 cycles of scan.

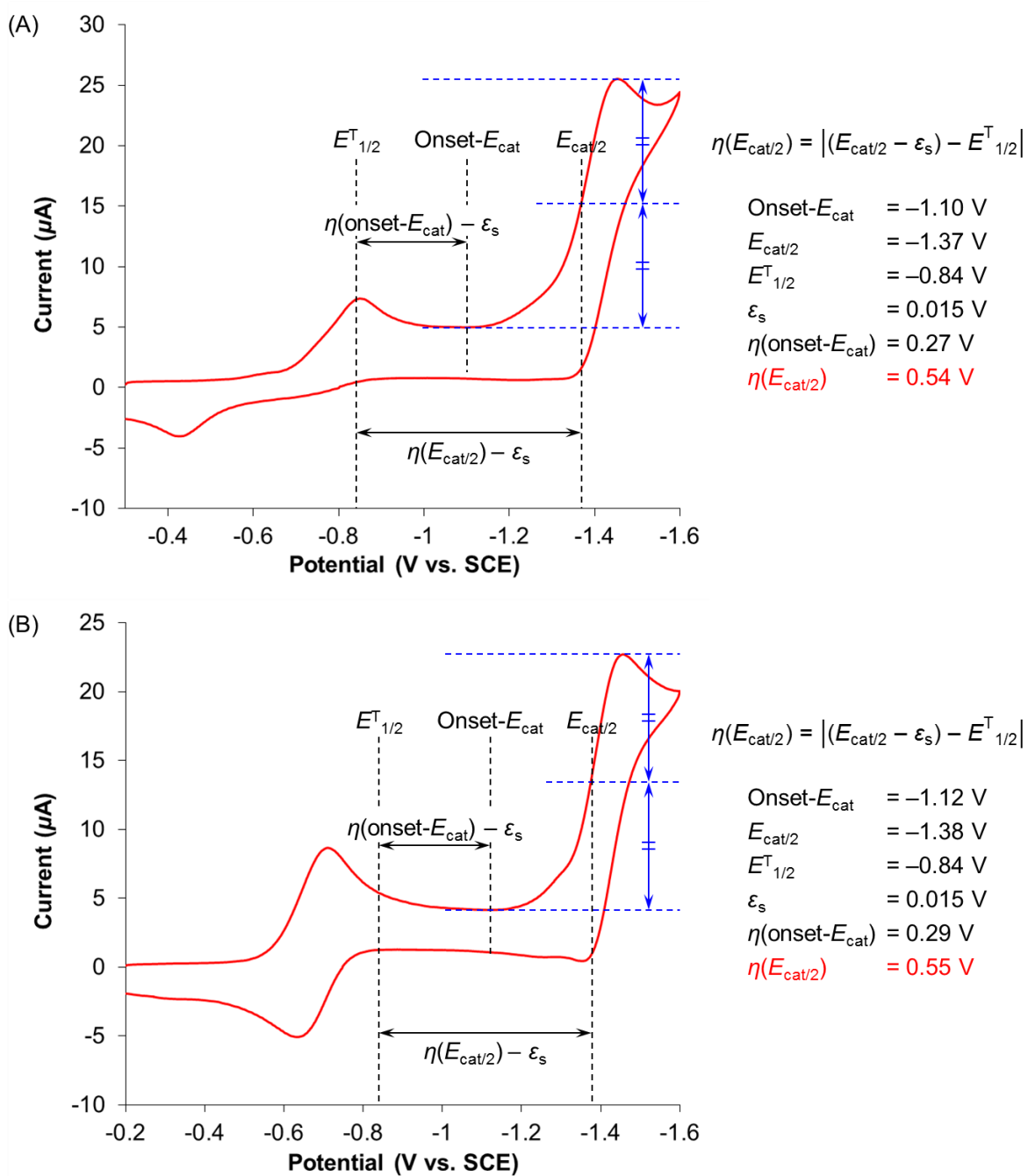


Fig. S22 Cyclic voltammograms of 1.0 mM (A) $[\text{CoCp}^*_2][\mathbf{1b}]$, (B) $[\text{CoCp}^*_2][\mathbf{2b}]$ and (C) $[\text{CoCp}^*_2][\mathbf{3b}]$ in DMF containing 0.10 M $n\text{-Bu}_4\text{NClO}_4$ as electrolyte and 10.0 mM AcOH using a glassy carbon working electrode, a platinum wire auxiliary electrode and a saturated calomel reference electrode at a scan rate of 50 mV/s.

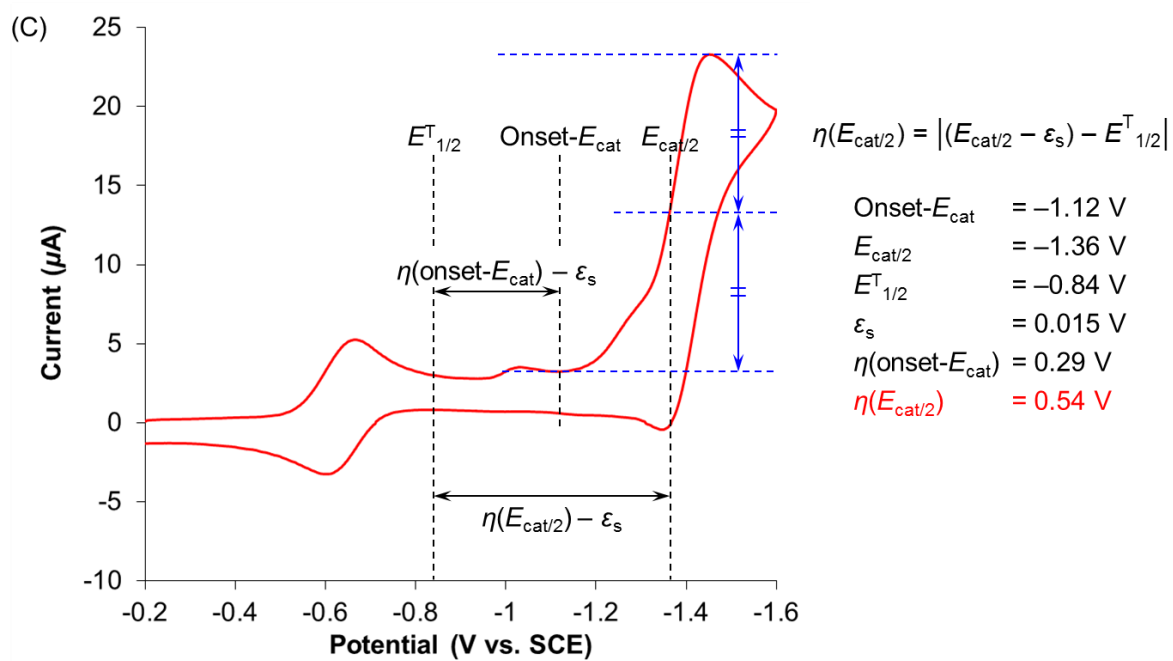


Fig. S22 (Continued)

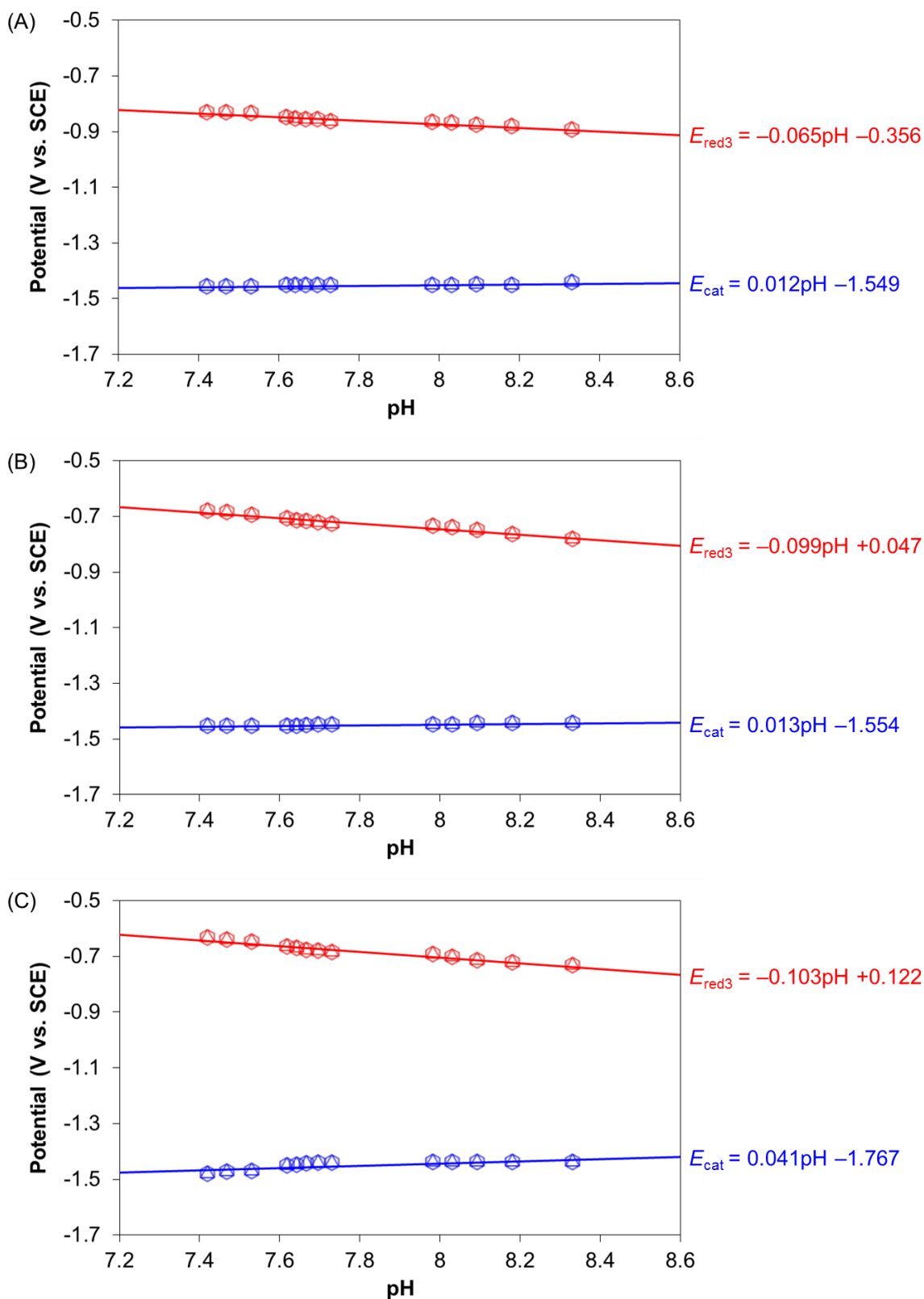


Fig. S22 Plots of peak potentials for first reduction and catalytic waves of (A) [CoCp*₂][**1b**], (B) [CoCp*₂][**2b**] and (C) [CoCp*₂][**3b**] vs. pH (Pourbaix diagram). Those potentials were determined by cyclic voltammetry of 1.0 mM [CoCp*₂][**1b**], [CoCp*₂][**2b**] and [CoCp*₂][**3b**] in DMF containing 0.10 M ⁿBu₄NClO₄ as electrolyte in the presence of various concentrations of AcOH using a glassy carbon working electrode, a platinum wire auxiliary electrode, and a saturated calomel reference electrode at a scan rate of 50 mV/s. pH values were estimated on the basis of a report by Smagowski et al.¹³

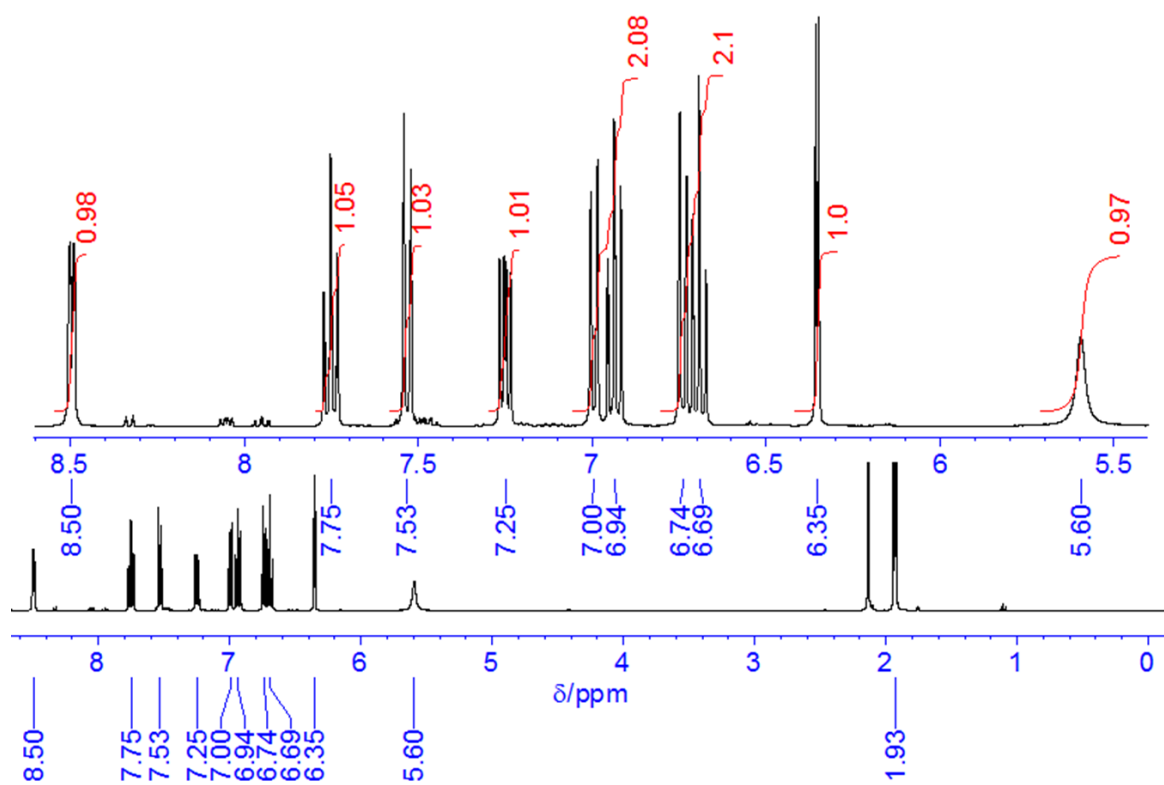


Fig. S23 ^1H NMR (400 MHz) spectrum of PyBtH_2 in CD_3CN .

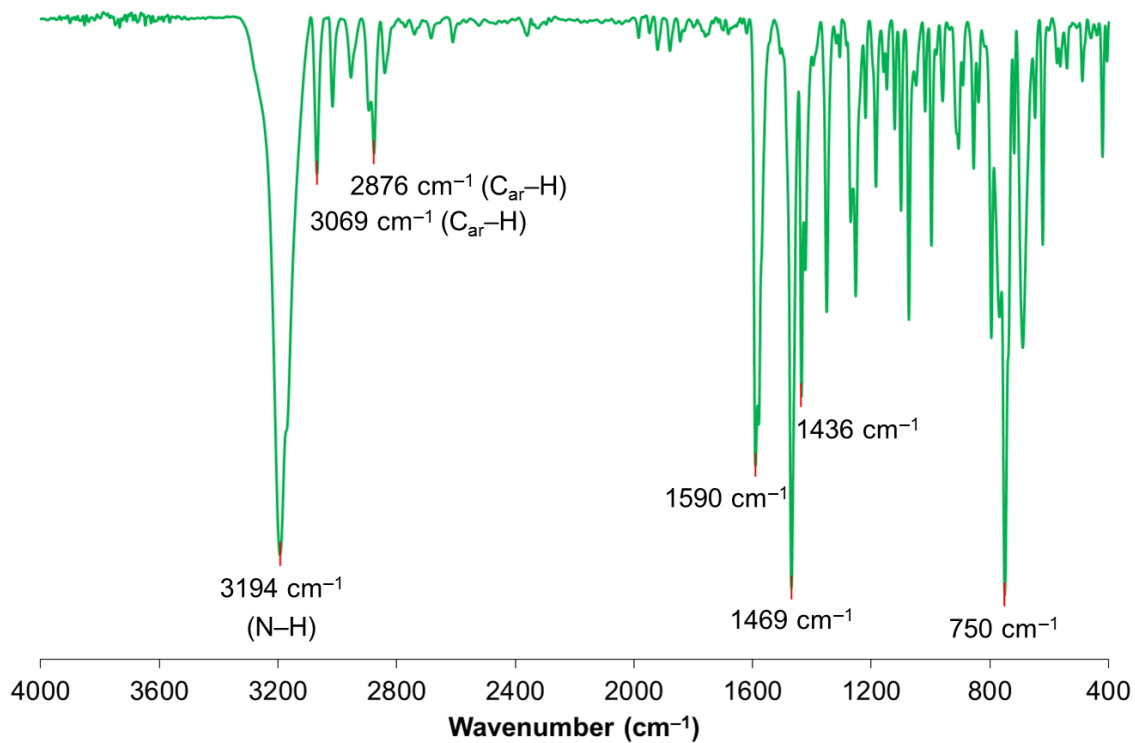


Fig. S24 FT-IR spectrum of PyBtH_2 in KBr disk.

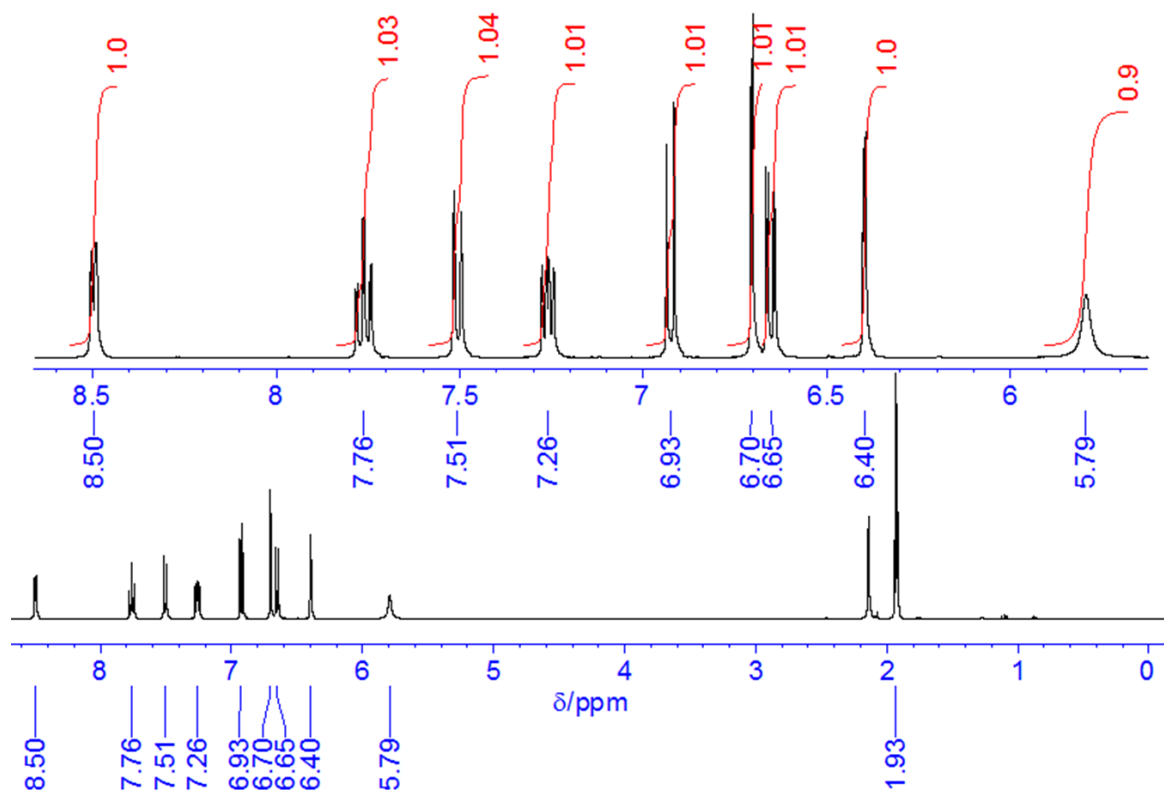


Fig. S25 ^1H NMR (400 MHz) spectrum of **PyCIBtH₂** in CD_3CN .

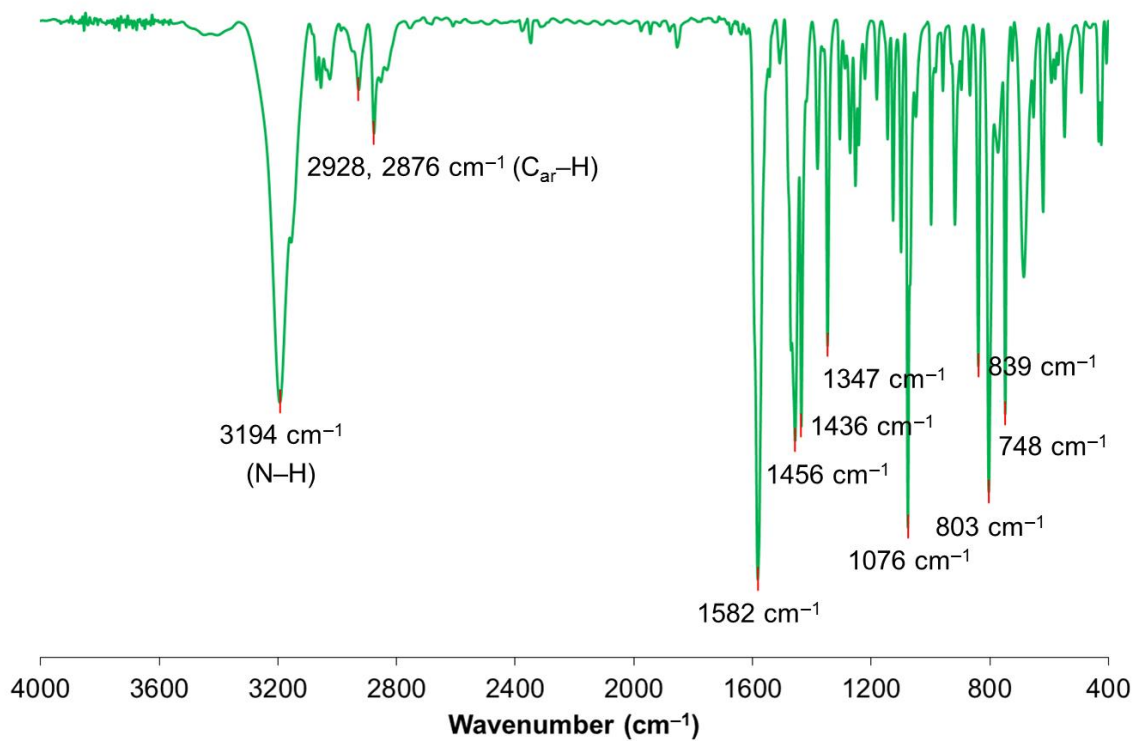


Fig. S26 FT-IR spectrum of **PyCIBtH₂** in KBr disk.

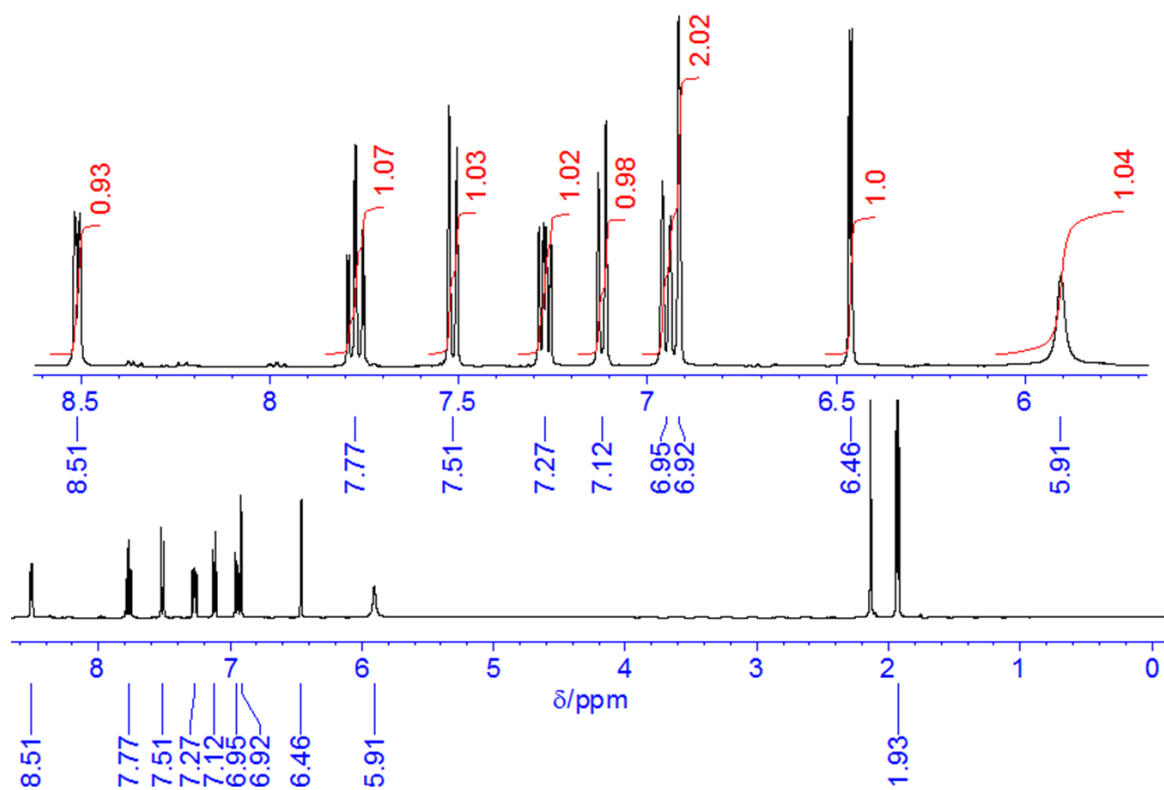


Fig. S27 ^1H NMR (400 MHz) spectrum of $\text{PyCF}_3\text{BtH}_2$ in CD_3CN .

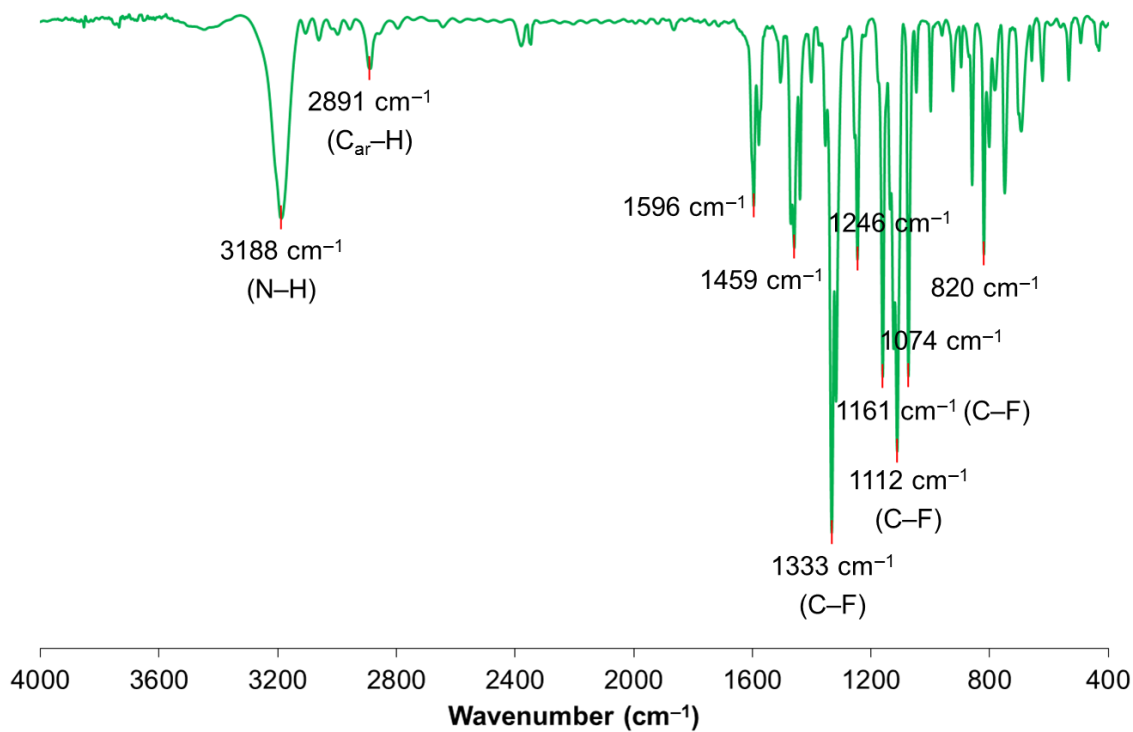


Fig. S28 FT-IR spectrum of $\text{PyCF}_3\text{BtH}_2$ in KBr disk.

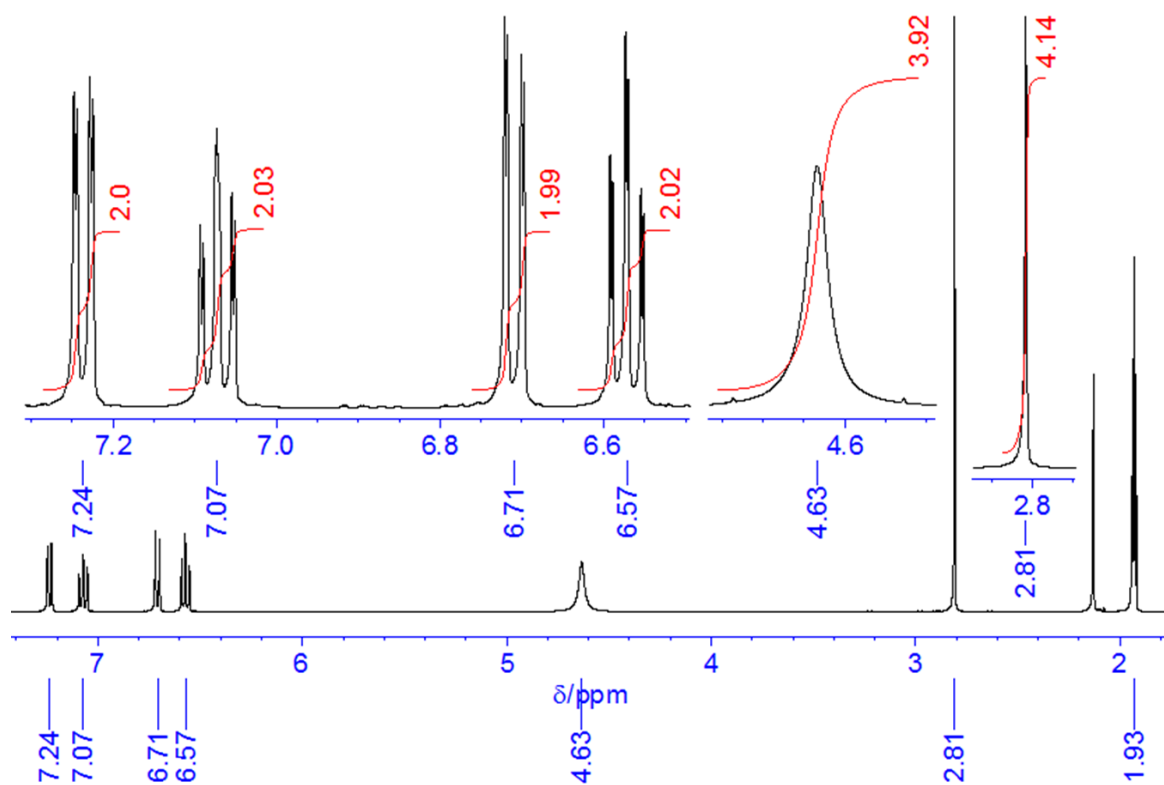


Fig. S29 ^1H NMR (400 MHz) spectrum of **BAPTE** in CD_3CN .

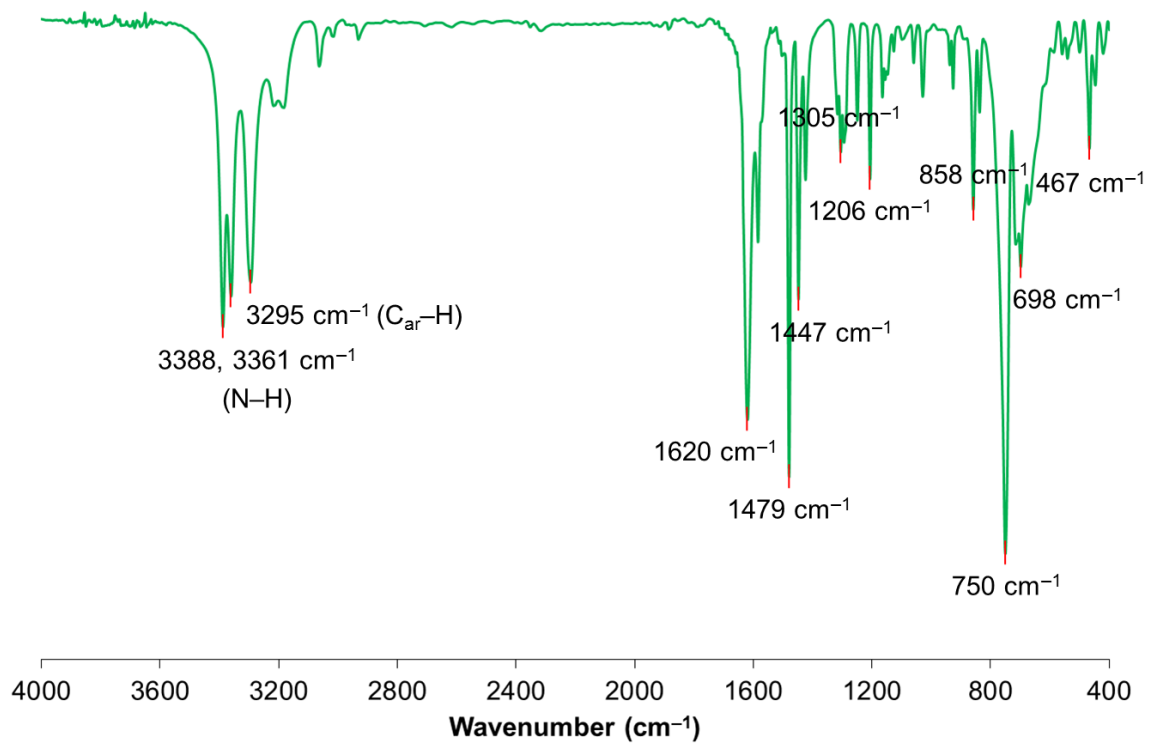


Fig. S30 FT-IR spectrum of **BAPTE** in KBr disk.

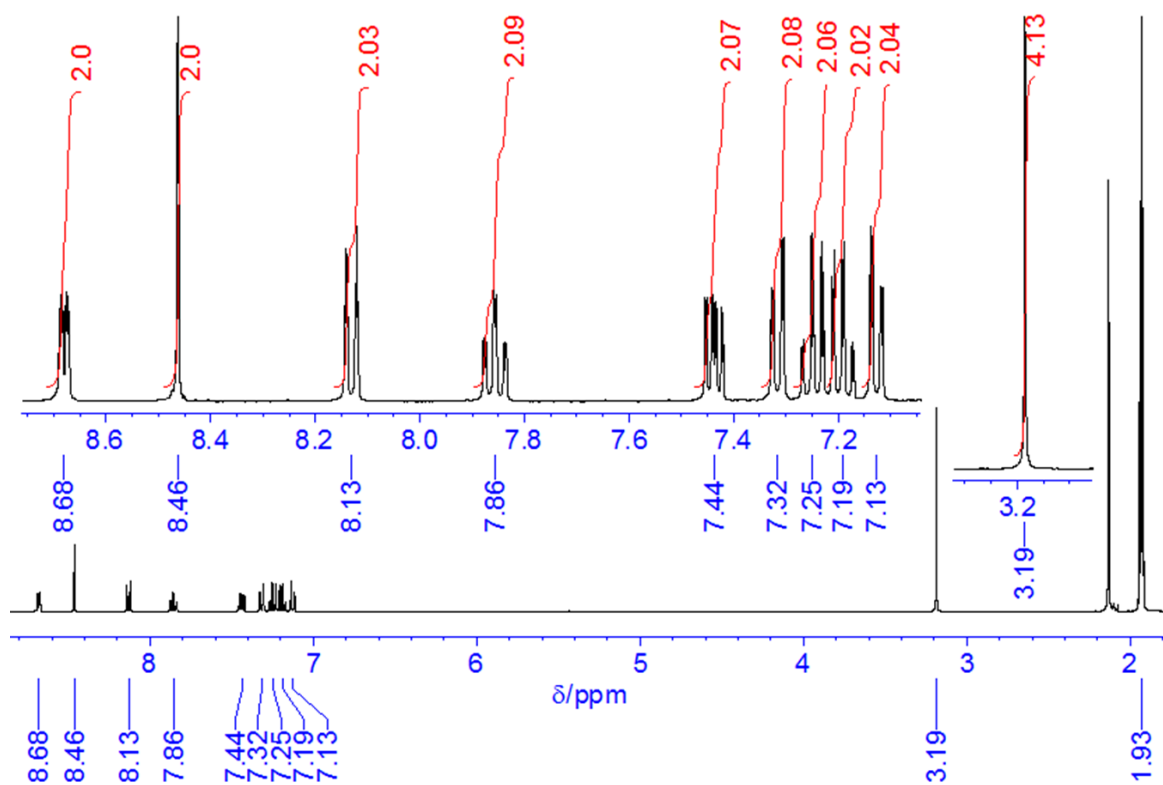


Fig. S31 ¹H NMR (400 MHz) spectrum of **BPAPTE** in CD₃CN.

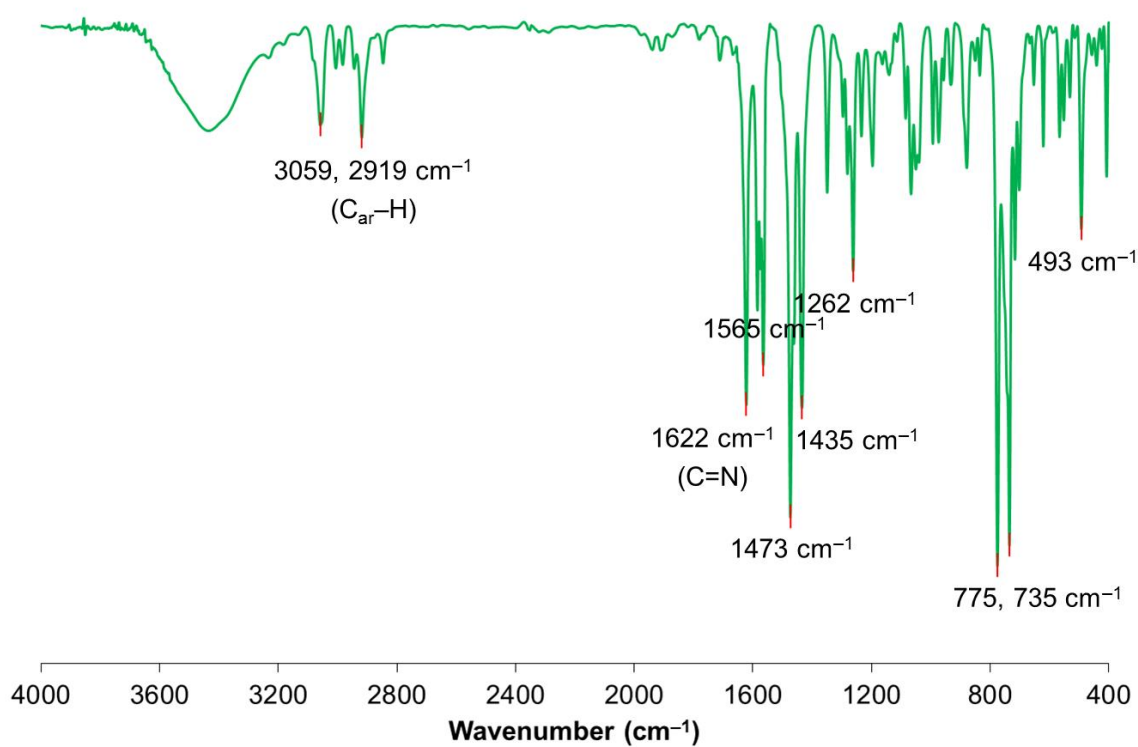


Fig. S32 FT-IR spectrum of **BPAPTE** in KBr disk.

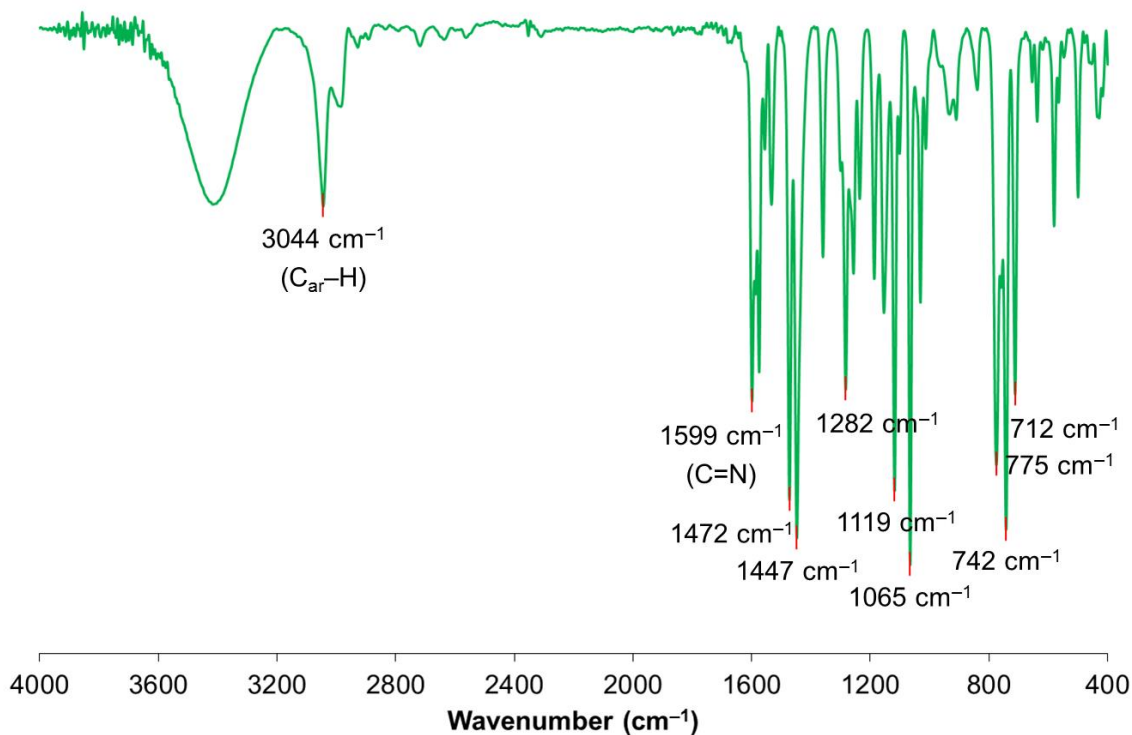


Fig. S33 FT-IR spectrum of **1a** in KBr disk.

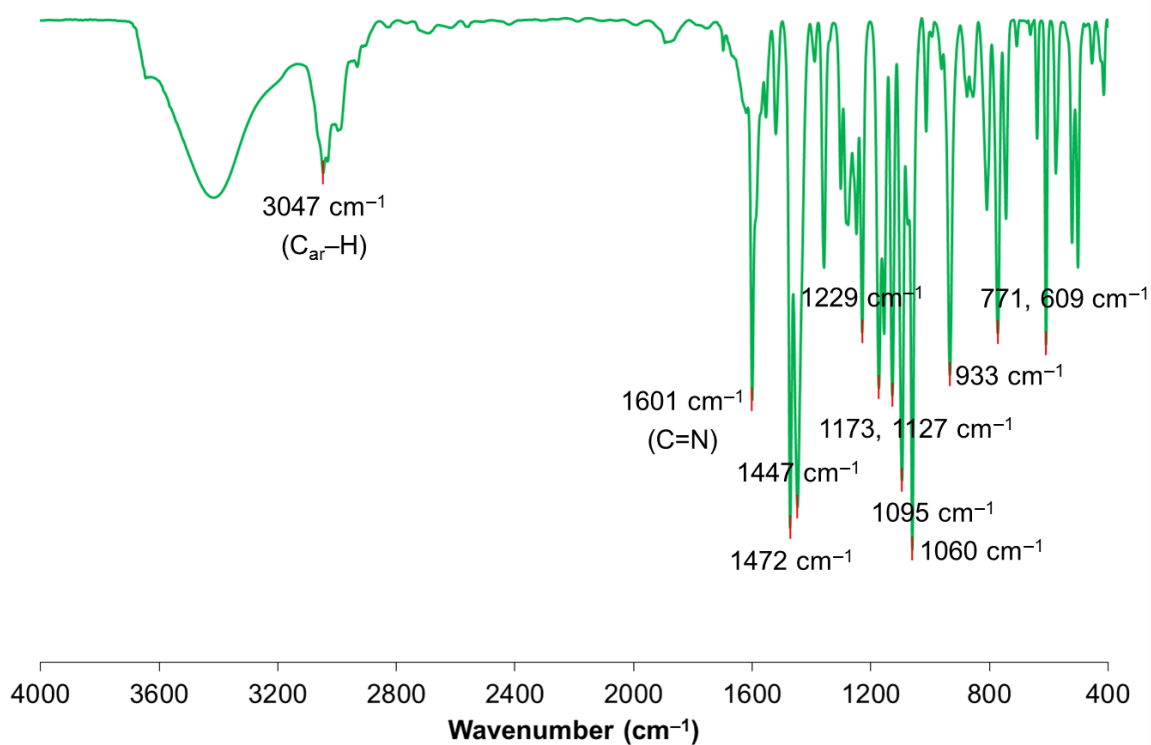


Fig. S34 FT-IR spectrum of **2a** in KBr disk.

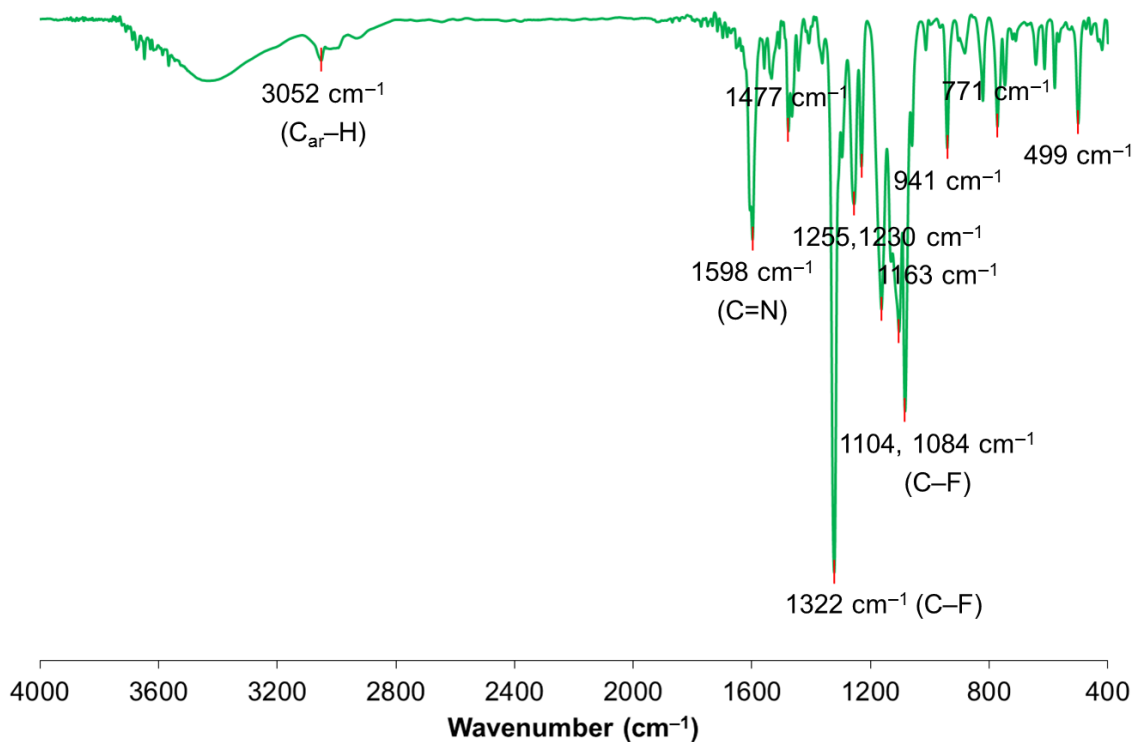


Fig. S35 FT-IR spectrum of **3a** in KBr disk.

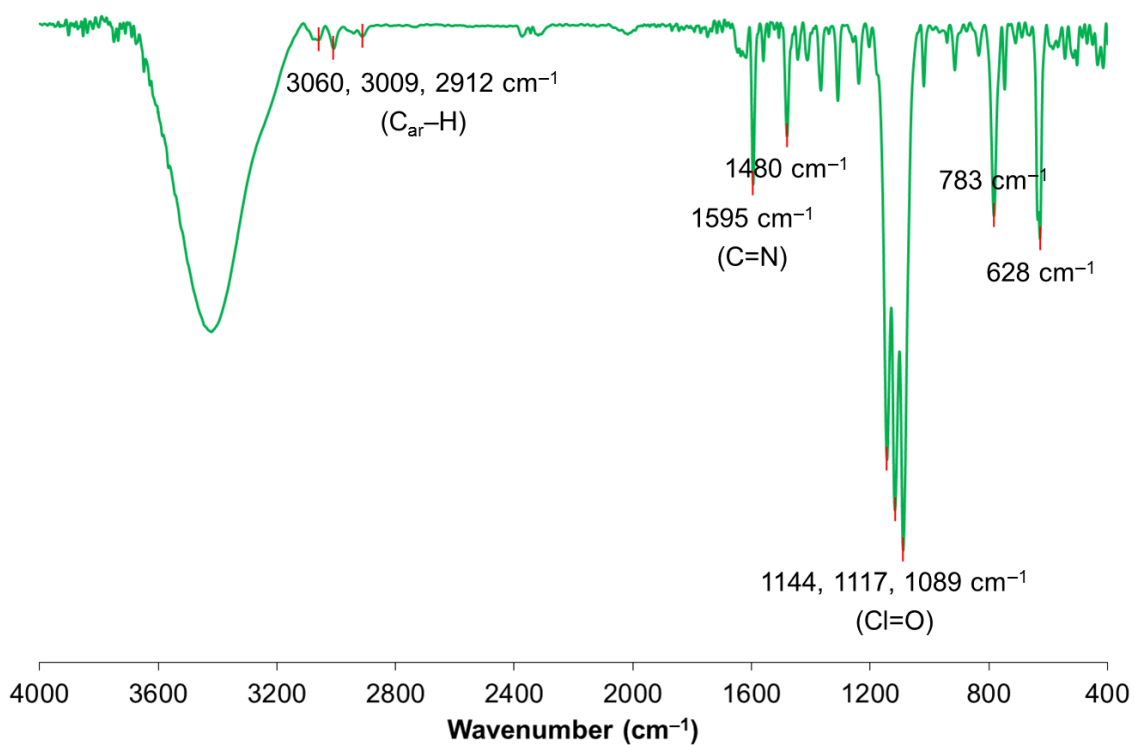


Fig. S36 FT-IR spectrum of **[5](ClO₄)₂** in KBr disk.

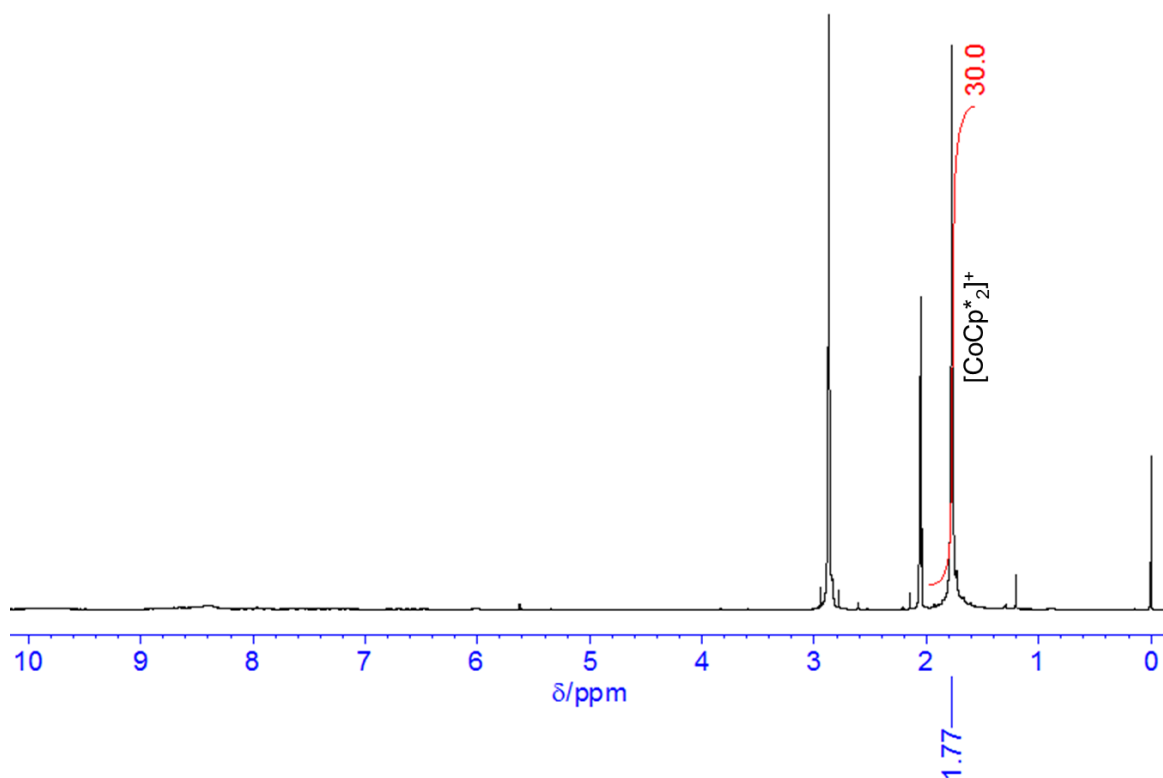


Fig. S37 ^1H NMR (400 MHz) spectrum of $[\text{CoCp}^*_2][\mathbf{1b}] \cdot 0.5\text{CH}_2\text{Cl}_2$ in acetone- d_6 .

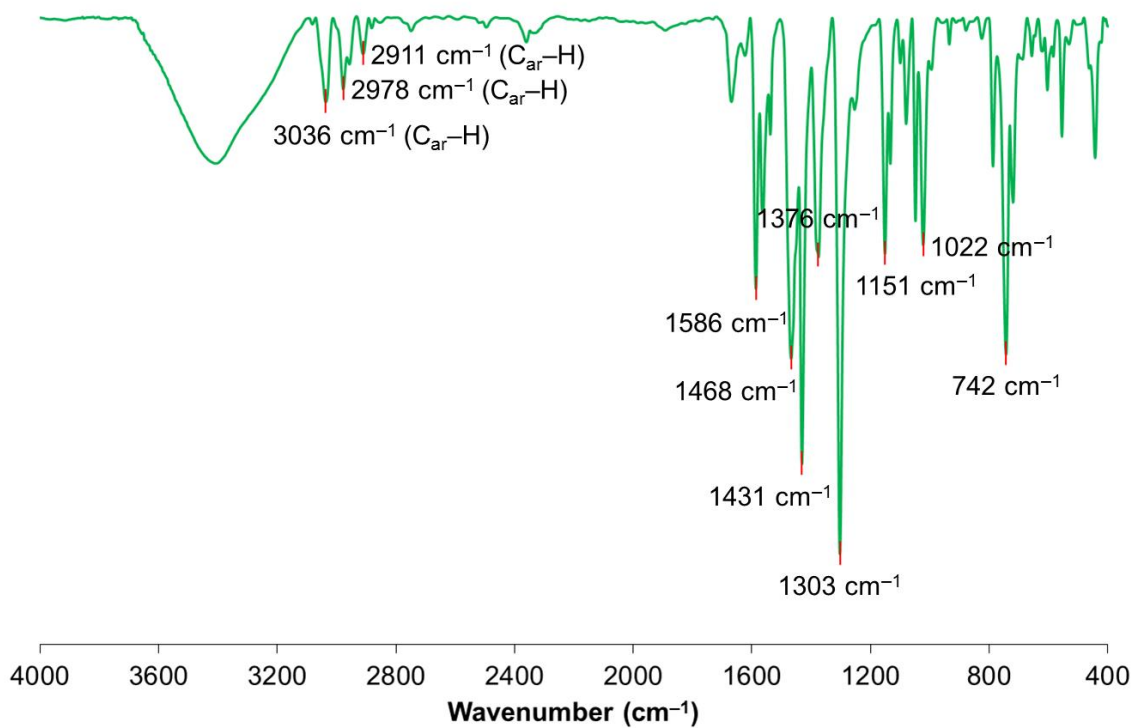


Fig. S38 FT-IR spectrum of $[\text{CoCp}^*_2][\mathbf{1b}] \cdot 0.5\text{CH}_2\text{Cl}_2$ in KBr disk.

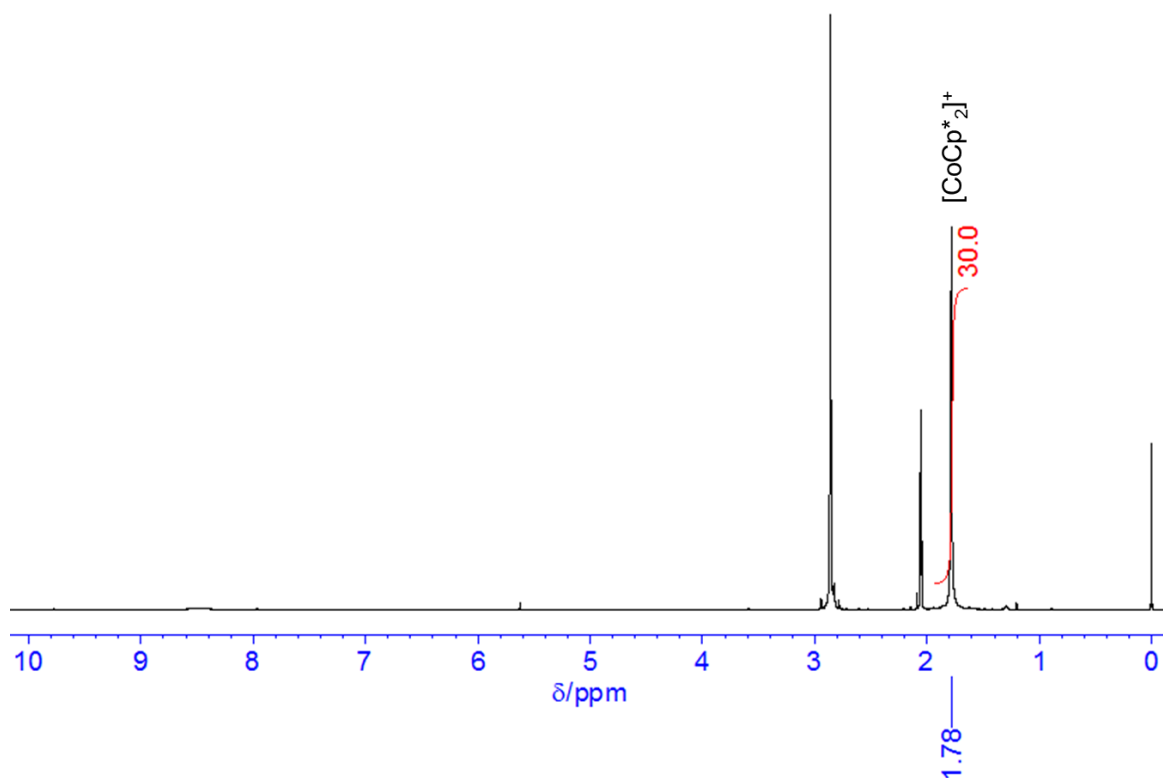


Fig. S39 ^1H NMR (400 MHz) spectrum of $[\text{CoCp}^*_2][\mathbf{2b}] \cdot 0.5\text{CH}_2\text{Cl}_2$ in acetone- d_6 .

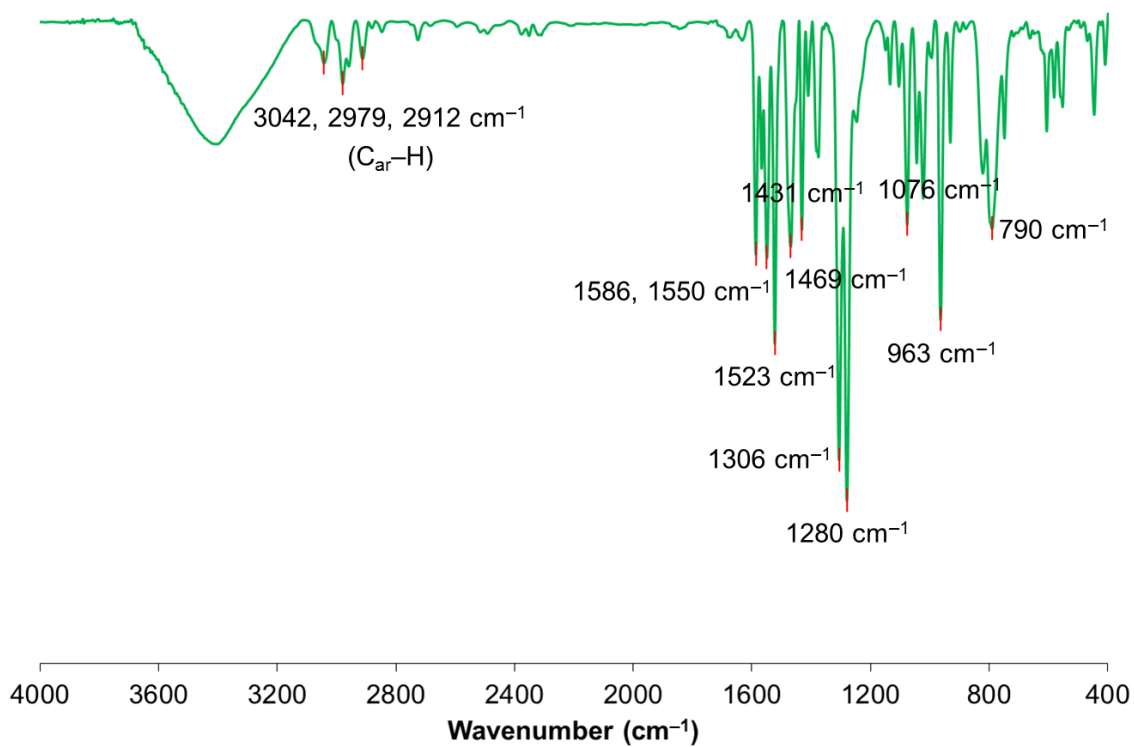


Fig. S40 FT-IR spectrum of $[\text{CoCp}^*_2][\mathbf{2b}] \cdot 0.5\text{CH}_2\text{Cl}_2$ in KBr disk.

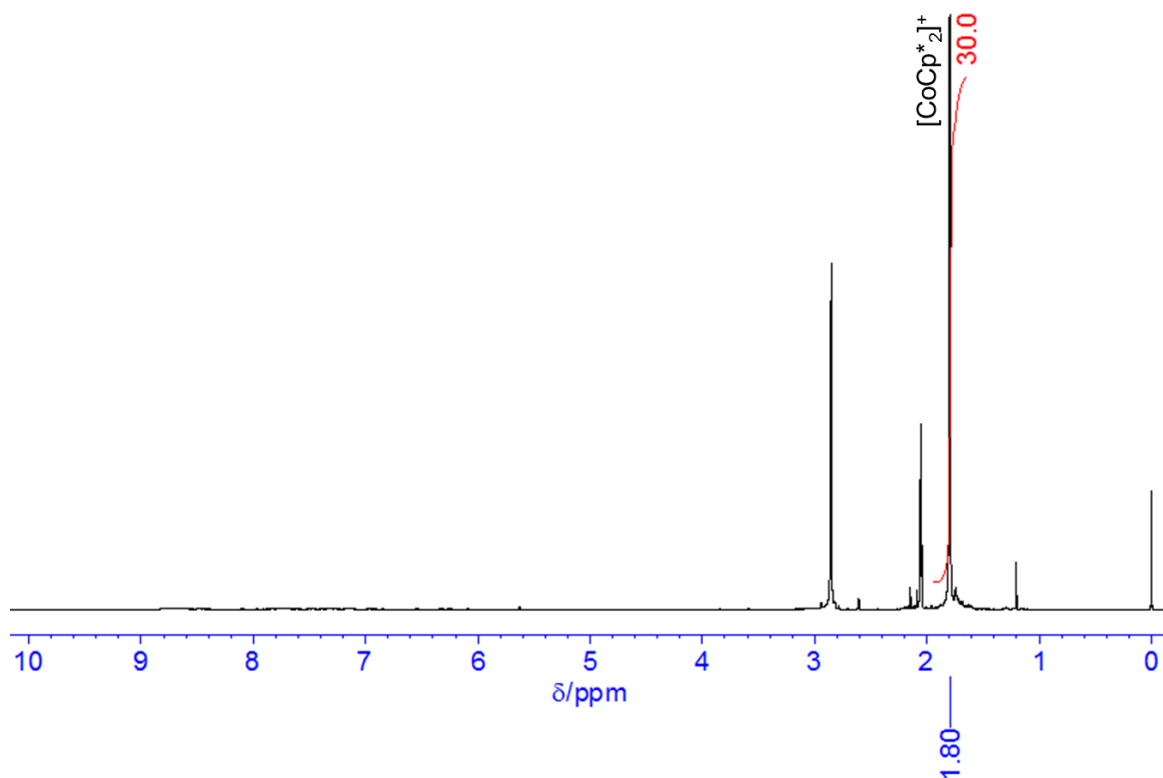


Fig. S41 ^1H NMR (400 MHz) spectrum of $[\text{CoCp}^*_2][\mathbf{3b}] \cdot 0.3\text{CH}_2\text{Cl}_2$ in acetone- d_6 .

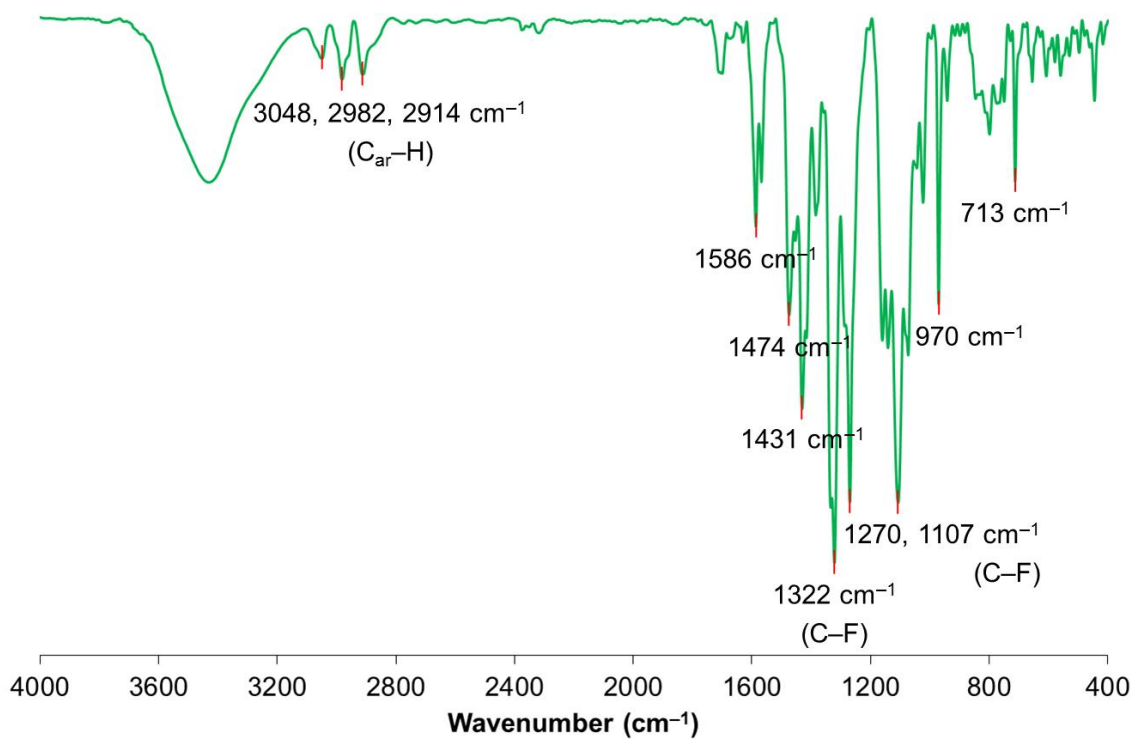


Fig. S42 FT-IR spectrum of $[\text{CoCp}^*_2][\mathbf{3b}] \cdot 0.3\text{CH}_2\text{Cl}_2$ in KBr disk.

REFERENCES

- 1 S. Inoue, M. Mitsuhashi, T. Ono, Y.-N. Yan, Y. Kataoka, M. Handa, T. Kawamoto, *Inorg. Chem.*, 2017, **56**, 12129–12138.
- 2 M. S. Lowry, W. R. Hudson, R. A. J. Pascal, S. Bernhard, *J. Am. Chem. Soc.*, 2004, **126**, 14129–14135.
- 3 S. K. Chatterjee, S. Roy, S. K. Barman, R. C. Maji, M. M. Olmstead, A. K. Patra, *Inorg. Chem.*, 2012, **51**, 7625–7635.
- 4 (a) M. C. Burla, R. Caliendo, M. Camalli, B. Carrozzini, G. L. Casciarano, L. De Caro, C. Giacovazzo, G. Polidori, R. Spagna, *J. Appl. Cryst.*, 2005, **38**, 381–388; (b) M. C. Burla, R. Caliendo, M. Camalli, B. Carrozzini, G. L. Casciarano, L. De Caro, C. Giacovazzo, G. Polidori, D. Siliqi, R. Spagna, *J. Appl. Cryst.*, 2007, **40**, 609–613.
- 5 (a) G. M. Sheldrick, *Acta Cryst. A*, 2014, **70**, C1437; (b) G. M. Sheldrick, *Acta Cryst. A*, 2008, **64**, 112–122.
- 6 Crystal Structure Analysis Package, Rigaku Corporation (2000–2018). Tokyo 196-8666, Japan.
- 7 N. H. Buttrus, S. A. Ahmed, W. M. Jameel, *Res. J. Chem. Sci.*, 2013, **3**, 47–54.
- 8 A. Kakanejadifard, T. Hayati, A. Rezayat, *Phosphorus, Sulfur, and Silicon*, 2010, **185**, 1511–1515.
- 9 H. N. Kagalwala, D. N. Chirdon, I. N. Mills, N. Budwal, S. Bernhard, *Inorg. Chem.*, 2017, **56**, 10162–10171.
- 10 G. Park, S. Y. Yi, J. Jung, E. J. Cho, Y. You, *Chem. Eur. J.*, 2016, **22**, 17790–17799.
- 11 S.-H. Wu, J.-W. Ling, S.-H. Lai, M.-J. Huang, C. H. Cheng, I.-C. Chen, *J. Phys. Chem. A*, 2010, **114**, 10339–10344.
- 12 J. Ciccione, N. Leconte, D. Luneau, C. Philouze, F. Thomas, *Inorg. Chem.*, 2016, **55**, 649–665.
- 13 I. M. Kolthoff, M. K. Chantooni, Jr, H. Smagowski, *Anal. Chem.*, 1970, **42**, 1622–1628.